REPORT NO.
UCB/SEMM-87/10

STRUCTURAL ENGINEERING
MECHANICS AND MATERIALS

INTERACTION BETWEEN HIGH-SPEED MOVING VEHICLES AND FLEXIBLE STRUCTURES: AN ANALYSIS WITHOUT ASSUMPTION OF KNOWN VEHICLE NOMINAL MOTION

BY

LOC VU-QUOC and MATS OLSSON

DECEMBER 1987

DEPARTMENT OF CIVIL ENGINEERING
UNIVERSITY OF CALIFORNIA
BERKELEY, CALIFORNIA

Interaction between High-Speed Moving Vehicles and Flexible Structures: An Analysis without Assumption of Known Vehicle Nominal Motion

By

L. Vu-Quoc† and M. Olsson‡

Abstract

Traditionally, in analyses of vehicle/structure interaction, especially when a vehicle mass comes in direct contact with the structure, vehicle nominal motion is often prescribed a-priori, and therefore unaffected by the structure flexibility. In this paper, a methodology is proposed in which this restriction is removed, allowing the vehicle nominal motion to become unknown, and encompassing the traditional approach as a particular case. General nonlinear equations of motion of a building-block model, applicable to both wheel-on-rail and magnetically levitated vehicles, are derived. These equations are simplified to a set of mildly nonlinear equations upon introducing additional assumptions — essentially on small structural deformation. Efficient and reliable predictor/corrector algorithms are proposed to integrate the nonlinear, coupled, spatially-discrete equations of motion. Several examples are given to illustrate the present formulation.

Table of Contents

† Applied Mechanics Division, Stanford University, Stanford, CA 94305.

‡ Division of Structural Mechanics, Lund University, Sweden. Presently visiting Structural Engineering, Mechanics, and Material Division, University of California, Berkeley, CA 94720.

December 10, 1987

Interaction between High-Speed Moving Vehicles and Flexible Structures: An Analysis without Assumption of Known Vehicle Nominal Motion

By

L. Vu-Quoc and M. Olsson

1. Introduction

In recent years considerable interest has been developed in implementing energy-efficient, high-speed, low-noise systems of transportation for airport-city or inter-city commuting — in particular magnetically levitated (Maglev) vehicle systems. A report on the status of development of these systems can be found for example in Eastham & Hayes [1987]. The speed of a Maglev vehicle can reach 400 to 500 km/h with a noise level comparable to that of a wheel-on-rail vehicle at 200 km/h. In the future, the efficiency of Maglev systems will increase manyfold as a result of advances in superconductor research. Currently, to ensure success of such systems, guideway structures must be designed to be stiff so that deflections remain within narrow margins of tolerance.§ The cost of a stiff guideway system can easily exceed 70% of the total cost of a system (Lawton [1985], Zicha [1986]). More flexible guideways — with fundamental frequency typically between 1 Hz and 6 Hz — are less expensive, but present complex vehicle/structure interaction. Progress in suspension control technology will, however, make possible the use of flexible guideways. The interaction between high-speed moving vehicles and flexible supporting structures is the focus of the present work. Even though the impetus behind this research is geared toward high-speed vehicles, the problem of moving loads does find applications in various fields of engineering, from transportation, naval architecture, to aeronautics and astronautics (see, e.g., Frýba [1972], Blejwas *et al* [1979] and references therein).

§ Deflection must fall approximately within $\pm 0.006m$ for a span of $L = 25m$, i.e., the deflection is about $L/4000$ (Emsland test track, Zicha [1986]).

Extensive lists of references on the subject of moving loads over elastic structures are contained in several review papers: Huang [1976], Kortüm & Wormley [1981], Ting *et al* [1975-83], report of Subcommittee on Vibration Problems [1985], Kortüm [1986]. The monograph by Frýba [1972] is the classical source of information on this subject. Formulation of the vehicle/structure interaction for wheel-on-rail vehicles or for Maglev vehicles with tight gap control leads to complex system of equations of motion. This complexity stems mainly from the constraints between a moving mass and the flexible guideway that must be maintained throughout the motion. Such problem does not arise for vehicle models connected to the structure via suspension systems where there is no constraint between a moving mass and the structure. Moreover, time derivatives of a function dependent on current position of the vehicle contain convective terms which become prominent at high speed regime. Analytical solution is possible only if the convective terms are neglected (Stanisic [1985]). The importance of these convective terms was amply demonstrated in Blejwas, Feng & Ayre [1979], where numerical results corroborated experimental findings. So far, research effort has been based on the assumption that vehicle nominal motion is known a-priori (e.g., Ting, Genin & Ginsberg [1974], Venancio-Filho [1978], Olsson [1985-86], Wallrapp [1986]). Since mathematical models in these work require prescribed vehicle nominal motion and do not admit driving forces, there is no possibility to study effects of structure flexibility on vehicle motion, or effects of applied accelerating or braking forces on the vehicle/structure system. We have not come across any reference where the assumption of known vehicle nominal motion is not used. In addition, efficient numerical algorithms must be developed to deal with the resulting complex system of equations of motion.

We propose herein a methodology to analyze the complete vehicle/structure interaction, valid for high speed regime, and without resorting to the usual assumption of known nominal motion. This general setting clearly includes the case where nominal motion is prescribed a-priori. The scope of this paper is restricted, however, to the basic

model of planar motion of a rigid wheel (rolling without slipping) or a Maglev magnet unit with tight gap control moving over a flexible beam. Energy-dissipative mechanisms such as structural damping, mechanical friction, or aerodynamic drag are not considered here.† The present prototype model will serve as a basic building block for more complex vehicle/structure models. We note that the wheel model finds also application in electrodynamic (repulsive) Maglev vehicles (see Kortüm & Wormley [1981] for a Maglev vehicle model with wheel sets), since these systems move on wheels up to a maximum lift-off speed of about $80km/h$ (Alscher *et al* [1983]). Further, both high-speed Maglev vehicles and wheel-on-rail vehicles may possibly run on the same bivalent guideway structure (Raschbichler & Wackers [1987]).

First, nonlinear equations of motion of the basic model, valid for large deformation of the beam, are derived for a class of general (nonlinear) contact constraints via Hamilton's principle of stationary action. The ability to account for large structural displacements is essential to analyze moving loads on very flexible structures, such as cable suspension systems, and in a broad range of dynamic response. In the present work, structural response in the small deformation range is, however, our main interest. With assumptions of small deformation, the nonlinear equations of motion are reduced, in a consistent manner, to a system of mildly nonlinear equations. This consistency is an important feature that distinguishes the present approach from traditional practice of complete linearization: Relevant nonlinear terms, essential for high speed regime, are retained in the equation for vehicle motion.

Galerkin method, in particular with finite-element basis functions, is employed to spatially discretize the equations for structural motion.‡ The result is a set of differential/algebraic equations (DAE's) in time. In addition to the convective terms, as given in Venancio-Filho [1978] and Olsson [1985] for a particular case of a point mass,

† See Cherchas [1979] for an example of modelling aerodynamic drag on high-speed vehicles.

‡ Green's function method as used by Ting, Genin & Ginsberg [1974] is not easily generalized to complex structures and boundary conditions.

the semi-discrete equations for structural motion contain terms of geometric nature. Integration algorithms for DAE have been proposed by several authors. However, Führer [1986] noted that when dealing with vehicle system dynamics (and without interaction with flexible structure), where equations of motion are DAE's, existing algorithms for DAE's (e.g., Petzold [1982]) may encounter serious problems. Consequently, transformation of DAE's of vehicle motion into the first order form of ordinary differential equations (ODE's) is the most reliable solution procedure.

In this work, we propose predictor/corrector methods for solving the system of DAE's derived from our formulation. These methods are also applicable to the general situation involving with complex vehicle models. In this general situation, the equations for vehicle motion are reliably solved using linear multi-step methods with variable step size and order. These are also very effective methods for solving stiff ODE's (see Gupta, Sacks-Davis & Tischer [1983]), often encountered in vehicle models. The equations for structural motion are solved by efficient step-by-step implicit algorithms for second order ODE's arised in structural dynamics. Note that the stiffness of these ODE's increases as one refines the spatial discretization of the partial differential equations (PDE's) for structural motion.† The implicit character of theses algorithms makes them effective tools for stiff systems in structural dynamics. Accuracy in structural motion are retained by not truncating these equations into a reduced-order model (projection onto an eigen-subspace). Further, these second order ODE's are not transformed into first order form as often done in vehicle dynamics program (see discussion in Kortüm [1986], Wallrapp [1986]). We thus maintain good accuracy in both vehicle motion and structural motion. In addition, our algorithms yield results that satisfy the essential balance of system energy. The present approach to vehicle/structure interaction, applicable to complex vehicle models, can be easily incorporated in existing vehicle dynamics programs, as well as in structural dynamics programs.

† We refer to Dekker & Verwer [1984] for discussions on stiffness of ODE's.

It should be noted that the study of dynamic motion of the complete system, driven by external forces, as done here is the only way to explain the Timoshenko paradox: Consider an example of a constant vertical force traversing, with some prescribed motion, a simply supported beam. Since the net work done by the force is zero, where does the energy which leaves the beam in a vibratory state after the traversing come from? The same question can be asked for a moving mass with prescribed motion. That is, it is not possible to check balance of energy in these models. In fact, the "excess" of energy comes precisely from the work done by external forces applied on the vehicle (cf. Maunder [1960]).

Several numerical examples are presented to show that effects of complete vehicle/structure interaction can possibly be evaluated with the present methodology. Soundness of the proposed algorithms is demonstrated in part by monitoring the offset of discrete energy balance of the system, introduced by error in the numerical results. We study the loss in velocity of a vehicle after traversing one or several spans of a continuous beam, as a result of energy transfer from the vehicle to the beam. Finally, we consider the braking of a vehicle, and its effects on the vehicle motion and the structural response.

2. Description of basic problem

In this section, we describe the kinematic assumptions employed in the basic problem of planar motion of a high-speed moving load — a single rigid wheel or a suspended magnet with tight gap control — over a flexible beam. Attention will be focused, however, to the dynamics of the more complex case of a rolling wheel. Several possible models of a Maglev magnet ("magnetic wheel") can be obtained from this basic model. Expressions of the kinetic energy and potential energy, which will be used later to derive the general nonlinear equations of motion, are also given. It should be kept in mind that this basic model serves as a building block for more complex vehicle/structure models.

2.1. Basic assumptions. Let $\{\mathbf{E}_1, \mathbf{E}_2\}$ be orthonormal basis vectors, and (X^1, X^2) the coordinates along these axes. These define the coordinate system of the material (undeformed) configuration. The line of centroids of the beam, of length L and initially straight, is assumed to lie along the axis $\mathbf{E}_1$; the coordinate of a material point on the line of centroids is denoted by $S \equiv X^1 \in [0, L]$. Let $\{\mathbf{e}_1, \mathbf{e}_2\}$ be the set of orthonormal vectors spanning the spatial (deformed) configuration, and conveniently chosen such that $\mathbf{E}_i \equiv \mathbf{e}_i$, for $i = 1,2$. The displacement of a material point S is denoted by $\mathbf{u}(S,t) = u^\alpha(S,t)\mathbf{e}_\alpha$,† where $t \in [0, +\infty)$ is the time parameter. Thus, u^1 is the axial displacement, and u^2 the transverse displacement of the beam centroidal line.

A rigid circular wheel — with (axi-symmetrically distributed) mass M, radius R, and rotatory inertia about center of mass I_w — is assumed to be in permanent contact with, and rolling without slipping on, the beam.‡ Let $\mathbf{Y}(t) = Y^\alpha(t)\mathbf{E}_\alpha$ be the position of the wheel center of mass in the undeformed configuration; its position in the spatial configuration is denoted by $\mathbf{y}(t) = y^\alpha(t)\mathbf{e}_\alpha$. We consider the following general form of (holonomic) contact constraints relating the position of the wheel ($\mathbf{Y}$ and $\mathbf{y}$) to the structural displacement ($\mathbf{u}$):

$$y^1(t) = Y^1(t) + g^1(\mathbf{u}(Y^1(t),t), \mathbf{u}_{,S}(Y^1(t),t)) , \tag{2.1a}$$

$$y^2(t) = Y^2(t) + g^2(\mathbf{u}(Y^1(t),t), \mathbf{u}_{,S}(Y^1(t),t)) , \tag{2.1b}$$

where $g^\alpha(\cdot,\cdot)$, $\alpha = 1,2$, are given functions of the structural displacement $\mathbf{u}$ and its spatial rate of change $\mathbf{u}_{,S} \equiv \dfrac{\partial \mathbf{u}}{\partial S} = \dfrac{\partial u^\beta}{\partial S}\mathbf{e}_\beta$, such that $g^\alpha(0, 0) \equiv 0$. We call $\mathbf{Y}(t)$, the motion of the wheel in the undeformed configuration of the beam, the *nominal motion* of the wheel. Given the functions $y^1(t)$, $\mathbf{u}(S,t)$, and $g^1(\mathbf{u}, \mathbf{u}_{,S})$, relation (2.1a) could be taken as a definition of the (unknown) nominal motion $Y^1(t)$, i.e., $Y^1(t)$ is defined to be a solution

† When the summation sign $\sum$ is omitted, summation convention is implied on the repeated indices, which take values in {1,2}.

‡ The velocity of the contact point on the wheel is only about (minus) one thousandth of the velocity of the wheel center of mass (rigid slip); see Kalker [1979].

of (2.1a). In this formulation, we consider only the case where $Y^2 \equiv \overline{R}$, for some constant $\overline{R}$. A defining property of the nominal motion should be noted: The nominal motion is identical to the spatial motion $\mathbf{y}$ when structural deformation is zero; that is, for $\mathbf{u}(S,t) \equiv 0$, we have $y^1(t) \equiv Y^1(t)$, and $y^2(t) = Y^2(t)$, since $g^\alpha(0, 0) = 0$. Let θ denote the angle of revolution of the wheel, which is considered to be a function of the nominal position Y^1 and the structural deformation $(\mathbf{u}, \mathbf{u}_{,S})$. Clearly, with $\mathbf{u}(S,t) = 0$ and for rolling motion without slipping, we have $\theta = Y^1/R$. We will often employ the shorthand notation $g^\alpha(Y^1,t) \equiv g^\alpha(\mathbf{u}(Y^1,t), \mathbf{u}_{,S}(Y^1,t))$, and similarly with $\theta(Y^1,t) \equiv \hat{\theta}(Y^1, \mathbf{u}(Y^1,t), \mathbf{u}_{,S}(Y^1,t))$. Thus,

$$\frac{\partial g^\alpha}{\partial S} \equiv \frac{\partial g^\alpha}{\partial u^\beta}\frac{\partial u^\beta}{\partial S} + \frac{\partial g^\alpha}{\partial u^\beta{}_{,S}}\frac{\partial^2 u^\beta}{\partial S^2}, \quad \frac{\partial \theta}{\partial S} \equiv \frac{\partial \hat{\theta}}{\partial S} + \frac{\partial \hat{\theta}}{\partial u^\beta}\frac{\partial u^\beta}{\partial S} + \frac{\partial \hat{\theta}}{\partial u^\beta{}_{,S}}\frac{\partial^2 u^\beta}{\partial S^2}. \tag{2.2}$$

2.2. Kinetic energy and potential energy. The expression of the kinetic energy K of the basic system (wheel and flexible beam) is given by

$$\begin{aligned} \mathcal{K} := \tfrac{1}{2}M\left\{ [\,\dot{Y}^1 + \dot{g}^1(Y^1,t)\,]^2 + [\,\dot{g}^2(Y^1,t)\,]^2 \right\} + \tfrac{1}{2}I_w[\dot{\theta}(Y^1,t)]^2 \\ + \tfrac{1}{2}\int_{[0,\,L]} A_\rho \left\{ [u^1{}_{,t}(S,t)]^2 + [u^2{}_{,t}(S,t)]^2 \right\} dS, \end{aligned} \tag{2.3}$$

where the superposed "$\cdot$" denotes the total time derivative, i.e., $\dot{(\cdot)} \equiv \frac{d}{dt}(\cdot)$; $u^\alpha{}_{,t} \equiv \frac{\partial u^\alpha}{\partial t}$ denotes the partial derivative in time, and A_ρ the mass per unit length of the beam.‡ Consider a function $f:[0, L]\times[0, \infty)\to\mathbb{R}$, smooth enough in both arguments. The first and second total time derivatives of $f(S,t)$, evaluated at $S = Y^1(t)$, are obtained as follows

$$\dot{f}(Y^1,\dot{Y}^1,t) = \frac{\partial f(Y^1,t)}{\partial S}\dot{Y}^1 + \frac{\partial f(Y^1,t)}{\partial t}, \tag{2.4a}$$

$$\ddot{f}(Y^1,\dot{Y}^1,\ddot{Y}^1,t) = \frac{\partial f(Y^1,t)}{\partial S}\ddot{Y}^1 + \frac{\partial^2 f(Y^1,t)}{\partial S^2}(\dot{Y}^1)^2 + 2\frac{\partial^2 f(Y^1,t)}{\partial S \partial t}\dot{Y}^1 + \frac{\partial^2 f(Y^1,t)}{\partial t^2}. \tag{2.4b}$$

‡ It should be noted that in (2.3) we do not consider the rotatory inertia of the beam cross-section; however, an analysis including this term could be carried out following the same methodology presented in this paper.

We will often omit to specify $(\dot{Y}^1, \ddot{Y}^1)$ in the argument list of quantities such as $\dot{f}$ and $\ddot{f}$, and write for instance $\dot{f}(Y^1,t) \equiv \dot{f}(Y^1,\dot{Y}^1,t)$ and $\ddot{f}(Y^1,t) \equiv \ddot{f}(Y^1,\dot{Y}^1,\ddot{Y}^1,t)$.§ Thus, employing (2.2) and (2.4) to evaluate $\dot{g}^\alpha(Y^1,t)$ (and later $\ddot{g}^\alpha(Y^1,t)$), one could obtain an expanded form of the total kinetic energy (2.3). The convective terms in (2.4) — i.e., the first term in (2.4a), and the first three terms in (2.4b) — play an important role in the interaction between high-speed moving vehicles and the supporting flexible structures, as shown in Blejwas, Feng & Ayre [1979]. These authors attributed to Ting, Genin & Ginsberg [1974] for recognizing this important effect. Further by the assumed smoothness of the function f in (2.4a-b), total time derivative and spatial derivative are interchangeable,

$$\frac{d^i}{dt^i}\left[\frac{\partial^j f(Y^1,t)}{\partial S^j}\right] = \frac{\partial^j}{\partial S^j}\left[\frac{d^i f(Y^1,t)}{dt^i}\right], \tag{2.4c}$$

and thus notation such as $\dot{f}_{,S}(Y^1,t)$ can be used without confusion.

The wheel is subjected to an applied force $\mathbf{F} = F^\alpha \mathbf{e}_\alpha$, and a torque T about its center of mass. Without loss of generality, the applied forces and torque can be considered, at the moment, as constant in time for the purpose of deriving the equations of motion. The work done by the external forces is then given by

$$W := \mathbf{F} \bullet \mathbf{y} + T\theta \,. \tag{2.5}$$

Let $\Psi(\mathbf{u})$ denote the elastic strain energy stored in the beam. The formulation is so far valid for large deformation in the beam, and we have not yet introduced assumptions of small deformation at this stage. Explicit expression of $\Psi(\mathbf{u})$ for finite deformation of a beam in plane motion can be found in Simo & Vu-Quoc [1986].

§ This shorthand notation has been used in (2.3).

3. Derivation of equations of motion

In this section, we derive the equations of motion for the basic system, valid for large structural deformation, by employing Hamilton's principle of stationary action. Additional assumptions of small deformation in the structure are subsequently introduced to further simplify the equations of motion. This simplification process is carefully carried out in a manner that is consistent with the assumptions. It should be indicated, however, that even though particularized to small structural deformation the resulting equations of motion do retain some crucial nonlinear terms, for an adequate description of the dynamics at high speed regime.

3.1. The general nonlinear equations of motion. The Lagrangian of the system can be written as

$$\mathbb{L}(Y^1,\mathbf{u}) := \mathbb{K}(Y^1,\mathbf{u}) - \Psi(\mathbf{u}) + W(Y^1,\mathbf{u}) \;. \ddagger \tag{3.1}$$

Consider the time interval $[t_1,t_2]$. Let $(\psi(t),\eta^1(S,t),\eta^2(S,t))$ be the admissible variations corresponding to the functions (Y^1,u^1,u^2), and vanishing at time $t = t_1$ and $t = t_2$. The equations of motion are obtained from the stationary condition of the action integral, i.e., the Euler-Lagrange equations corresponding to (3.1):

$$\frac{d}{d\epsilon}\int_{[t_1,\,t_2]} \mathbb{L}(Y^1+\epsilon\psi,\,\mathbf{u}+\epsilon\eta)dt\bigg|_{\epsilon=0} = 0\;, \tag{3.2}$$

for all admissible variations (ψ,η), where $\boldsymbol{\eta} = \eta^\beta \mathbf{e}_\beta$. It follows that the equations for nominal motion Y^1 and for structural displacement $\mathbf{u}$ are given by

$$\frac{d}{d\epsilon}\int_{[t_1,\,t_2]} \mathbb{L}(Y^1+\epsilon\psi,\,\mathbf{u})dt\bigg|_{\epsilon=0} = \frac{d}{d\epsilon}\int_{[t_1,\,t_2]} \mathbb{L}(Y^1,\,\mathbf{u}+\epsilon\eta)dt\bigg|_{\epsilon=0} = 0\;, \tag{3.3}$$

respectively, for all admissible variations (ψ,η).

---

‡ We omit the time derivatives of $(Y^1,\mathbf{u})$ in the argument list of $\mathbb{L}$ and $\mathbb{K}$ to alleviate the notation.

Nominal motion Y^1. We first note that from (2.4a) one has

$$\frac{\partial \dot{f}(Y^1,\dot{Y}^1,t)}{\partial \dot{Y}^1} \equiv \frac{\partial f(Y^1,t)}{\partial S} . \tag{3.4a}$$

Then, it follows from (3.4a) and (2.4c) that

$$\frac{d}{dt}\left[\frac{\partial \dot{f}(Y^1,t)}{\partial \dot{Y}^1}\right] = \frac{d}{dt}\left[\frac{\partial f(Y^1,t)}{\partial S}\right] \equiv \frac{\partial \dot{f}(Y^1,t)}{\partial S} . \tag{3.4b}$$

Further, the variation of f with respect to Y^1 is given by

$$\frac{d}{d\epsilon}\dot{f}(Y^1+\epsilon\psi,\, t)\bigg|_{\epsilon=0} = \frac{\partial \dot{f}(Y^1,t)}{\partial S}\,\psi + \frac{\partial f(Y^1,t)}{\partial S}\,\dot{\psi} , \tag{3.5}$$

where we have made use of (2.4a). Another way to obtain (3.5) is by interchanging $\frac{d}{d\epsilon}$ and $\frac{d}{dt}$, and then using (2.4c). Next, computing the directional derivative in $(3.3)_1$ together with integration by parts with respect to time, applying the boundary condition $\psi(t_1) = \psi(t_2) \equiv 0$, and then using (3.4) and (3.5) with $f \equiv g^\alpha$ to allow cancellation of certain terms, we obtain

$$-\frac{d}{d\epsilon}\int_{[t_1,\,t_2]} I\!K(Y^1+\epsilon\psi,\,\mathbf{u})dt\bigg|_{\epsilon=0} = \int_{[t_1,\,t_2]}\left\{M\left(1+\frac{\partial g^1(Y^1,t)}{\partial S}\right)[\ddot{Y}^1 + \ddot{g}^1(Y^1,t)]\right.$$

$$\left. + M\frac{\partial g^2(Y^1,t)}{\partial S}\,\ddot{g}^2(Y^1,t) + I_w\frac{\partial \theta(Y^1,t)}{\partial S}\,\ddot{\theta}(Y^1,t)\right\}\psi\, dt , \tag{3.6a}$$

$$\frac{d}{d\epsilon}\int_{[t_1,\,t_2]} W(Y^1+\epsilon\psi,\,\mathbf{u})dt\bigg|_{\epsilon=0} = \int_{[t_1,\,t_2]}\left\{F^1\left(1+\frac{\partial g^1(Y^1,t)}{\partial S}\right) + F^2\frac{\partial g^2(Y^1,t)}{\partial S} + T\frac{\partial \theta(Y^1,t)}{\partial S}\right\}\psi\, dt . \tag{3.6b}$$

The stationary condition $(3.3)_1$ and relations (3.6) yield the equation for the nominal motion Y^1:

$$M\left(1 + \frac{\partial g^1(Y^1,t)}{\partial S}\right)[\ddot{Y}^1 + \ddot{g}^1(Y^1,t)] + M\frac{\partial g^2(Y^1,t)}{\partial S}\ddot{g}^2(Y^1,t) + I_w\frac{\partial\theta(Y^1,t)}{\partial S}\ddot{\theta}(Y^1,t) =$$

$$F^1\left(1 + \frac{\partial g^1(Y^1,t)}{\partial S}\right) + F^2\frac{\partial g^2(Y^1,t)}{\partial S} + T\frac{\partial\theta(Y^1,t)}{\partial S}\,. \tag{3.7}$$

Structural motion (u^1,u^2). Similar to relations (3.4), one can prove that the following identities hold

$$\frac{\partial\dot{g}^\alpha(\mathbf{u},\mathbf{u}_{,S})}{\partial\dot{u}^\beta} \equiv \frac{\partial g^\alpha(\mathbf{u},\mathbf{u}_{,S})}{\partial u^\beta}\,, \quad \frac{d}{dt}\left(\frac{\partial\dot{g}^\alpha(\mathbf{u},\mathbf{u}_{,S})}{\partial\dot{u}^\beta}\right) \equiv \frac{\partial\dot{g}^\alpha(\mathbf{u},\mathbf{u}_{,S})}{\partial u^\beta}\,, \tag{3.8a}$$

$$\frac{\partial\dot{g}^\alpha(\mathbf{u},\mathbf{u}_{,S})}{\partial\dot{u}^\beta{}_{,S}} \equiv \frac{\partial g^\alpha(\mathbf{u},\mathbf{u}_{,S})}{\partial u^\beta{}_{,S}}\,, \quad \frac{d}{dt}\left(\frac{\partial\dot{g}^\alpha(\mathbf{u},\mathbf{u}_{,S})}{\partial\dot{u}^\beta{}_{,S}}\right) \equiv \frac{\partial\dot{g}^\alpha(\mathbf{u},\mathbf{u}_{,S})}{\partial u^\beta{}_{,S}}\,. \tag{3.8b}$$

Now, computation of the directional derivative in $(3.3)_2$, and integration by parts with respect to time yield the following results

$$-\frac{d}{d\epsilon}\int_{[t_1,t_2]} I\!K(Y^1,\mathbf{u}+\epsilon\boldsymbol{\eta})dt\Big|_{\epsilon=0} = \int_{[t_1,t_2]}\Big\{M\ddot{y}^\alpha\left(\eta^\beta(Y^1,t)\frac{\partial g^\alpha(Y^1,t)}{\partial u^\beta} + \eta^\beta{}_{,S}(Y^1,t)\frac{\partial g^\alpha(Y^1,t)}{\partial u^\beta{}_{,S}}\right)$$

$$I_w\ddot{\theta}(Y^1,t)\left(\eta^\beta(Y^1,t)\frac{\partial\theta(Y^1,t)}{\partial u^\beta} + \eta^\beta{}_{,S}(Y^1,t)\frac{\partial\theta(Y^1,t)}{\partial u^\beta{}_{,S}}\right) + \int_{[0,L]} A_\rho\eta^\beta u^\beta{}_{,tt}\,dS\Big\}dt\,, \tag{3.9a}$$

$$\frac{d}{d\epsilon}\int_{[t_1,t_2]} W(Y^1,\mathbf{u}+\epsilon\boldsymbol{\eta})dt\Big|_{\epsilon=0} = \int_{[t_1,t_2]}\Big\{F^\alpha\left(\eta^\beta(Y^1,t)\frac{\partial g^\alpha(Y^1,t)}{\partial u^\beta} + \eta^\beta{}_{,S}(Y^1,t)\frac{\partial g^\alpha(Y^1,t)}{\partial u^\beta{}_{,S}}\right)$$

$$+ T\left(\eta^\beta(Y^1,t)\frac{\partial\theta(Y^1,t)}{\partial u^\beta} + \eta^\beta{}_{,S}(Y^1,t)\frac{\partial\theta(Y^1,t)}{\partial u^\beta{}_{,S}}\right)\Big\}dt\,, \tag{3.9b}$$

where we have made use of the (homogeneous) boundary conditions of (η^1,η^2) at $t = t_1$ and $t = t_2$, relation (2.4a), and the identities (3.8). Note that we could also obtain these results by making use of the interchangeability of $\frac{d}{d\epsilon}$ and $\frac{d}{dt}$. Next, let the weak form of the stiffness operator be denoted by $G(\cdot,\cdot)$, and

$$G(\mathbf{u},\boldsymbol{\eta}) = \frac{d}{d\epsilon}\Psi(\mathbf{u} + \epsilon\boldsymbol{\eta})\Big|_{\epsilon=0}\,, \tag{3.10a}$$

where we recall that $\Psi(\mathbf{u})$ designates the strain energy of the beam. Expression of the

weak form $G(\mathbf{u},\eta)$ in the case of finite deformation of a beam in plane motion is given in Simo & Vu-Quoc [1986]. Therefore using $(3.3)_2$, (3.9) and (3.10a), the weak form of the structural equations of motion is then given by

$$\left(-F^1 + M[\ddot{Y}^1 + \ddot{g}^1(Y^1,t)]\right)\left(\eta^\beta(Y^1,t)\frac{\partial g^1(Y^1,t)}{\partial u^\beta} + \eta^\beta{}_{,S}(Y^1,t)\frac{\partial g^1(Y^1,t)}{\partial u^\beta{}_{,S}}\right)$$

$$+ \left(-F^2 + M\ddot{g}^2(Y^1,t)\right)\left(\eta^\beta(Y^1,t)\frac{\partial g^2(Y^1,t)}{\partial u^\beta} + \eta^\beta{}_{,S}(Y^1,t)\frac{\partial g^2(Y^1,t)}{\partial u^\beta{}_{,S}}\right)$$

$$+ \left(-T + I_w\ddot{\theta}(Y^1,t)\right)\left(\eta^\beta(Y^1,t)\frac{\partial\theta(Y^1,t)}{\partial u^\beta} + \eta^\beta{}_{,S}(Y^1,t)\frac{\partial\theta(Y^1,t)}{\partial u^\beta{}_{,S}}\right)$$

$$+ \int_{[0,\,L]} A_\rho\eta^\beta(S,t)\,u^\beta{}_{,tt}(S,t)dS + G(\mathbf{u},\eta) = 0\,,\quad \forall \text{ admissible } \eta\,,\dagger \tag{3.10b}$$

where $\beta = 1$ corresponds to the equation of motion for axial displacement u^1, and similarly $\beta = 2$ for transverse displacement u^2. The corresponding partial differential equations of motion can be easily obtained from (3.10) by integration by parts in S, and by invoking the fundamental theorem of calculus of variations.‡ We prefer, however, to retain the structural equations of motion in its weak form for subsequent numerical work.

3.2. Contact constraints and contact forces. Let $\bar{R}$ $(= Y^2)$ denote the distance from the beam centroidal line to the center of mass of the wheel. When $\bar{R} = R$, the wheel is moving with its circumference tangent to the beam centroidal line. Explicit form of the function g^α in the general constraint equations (2.1) for wheel/beam contact, or magnet/beam with constant gap (also referred to here as "contact" constraint), can be written exactly as follows

$$g^1(\mathbf{u},\,\mathbf{u}_{,S}) = u^1 - \bar{R}\sin\chi(\mathbf{u}_{,S})\,,\quad g^2(\mathbf{u},\,\mathbf{u}_{,S}) = u^2 - \bar{R}[1-\cos\chi(\mathbf{u}_{,S})]\,, \tag{3.11a}$$

$$\text{where}\quad \chi(\mathbf{u}_{,S}) := \tan^{-1}\left(\frac{u^2{}_{,S}}{1 + u^1{}_{,S}}\right), \tag{3.11b}$$

† Summation convention is implied on the repeated index $\beta \in \{1,2\}$.

‡ The containing space of the variations (η^1,η^2) should be suitably chosen and should include the boundary

represents the slope angle of the deformed beam (cf. Figure 3.1). It should be noted that the expressions in (3.11) are written for beam theory without shear deformation, and are valid for a finitely deformed beam.

Remark 3.1. "Magnetic wheel." The above formulation encompasses several possible models for a Maglev vehicle using electromagnetic suspension (attractive system) with tight gap control (see the review paper by Kortüm & Wormley [1981]).† By letting $I_w \equiv 0$ (or $\theta \equiv 0$) in the kinetic energy (2.3), we have a model (A) of a moving magnet, where $\bar{R}$ represents the distance from the beam centroidal line to the magnet center of mass. Next, by letting $I_w = \bar{R} \equiv 0$, in which case the constraints (2.1) becomes $y^1(t) = Y^1(t) + u^1(Y^1,t)$ and $y^2(t) = u^2(Y^1,t)$, we obtain yet another model (B) of a moving magnet. In practice, often even simpler constraints are chosen so that (model C) $y^1(t) \equiv Y^1(t)$ and $y^2(t) = u^2(Y^1,t)$ (cf., e.g., Wallrapp [1986]). Thus, there is no coupling between vehicle nominal motion and structural axial deformation. In this case, the equations of motion (3.7) and (3.10) (in weak form) simplify to

$$M[\ddot{Y}^1 + \frac{\partial u^2(Y^1,t)}{\partial S}\,\ddot{u}^2(Y^1,t)] = F^1 + F^2\frac{\partial u^2(Y^1,t)}{\partial S}\,, \tag{3.12a}$$

$$\eta^2(Y^1,t)[-F^2 + M\ddot{u}^2(Y^1,t)] + \int_{[0,\,L]} A_\rho \eta^\beta(S,t)\, u^\beta{}_{,tt}(S,t)dS + G(\mathbf{u},\eta) = 0\,,\ddagger \tag{3.12b}$$

which are also valid for a finitely deformed beam. In (3.12), the equation for axial displacement and the equation for transverse displacement are coupled through the nonlinear nature of $G(\mathbf{u},\eta)$ in the finite deformation case. Discussion on the difference between these models is postponed until we had introduced the small deformation assumptions and the simplified equations of motion in the coming sub-sections. □

---

conditions at $S = 0$ and $S = L$ (see, e.g., Rektorys [1980]).

† The gap between a magnet and the guideway is in the range of 10-15 mm, independently of vehicle speed (Eastham & Hayes [1987]).

‡ Summation convention is implied on the repeated index $\beta \in \{1,2\}$.

In the design of flexible structures under moving vehicles, it is important to quantify the (dynamic) contact forces transferred from a vehicle to the supporting structure. Further, the evaluation of these contact forces is crucial in the study of structure response under acceleration or braking action of a moving vehicle. Note that the governing longitudinal force for the design of guideways corresponds to that produced in an emergency braking. For the basic problem considered herein, let $\mathbf{F}_c = F_c^\alpha \mathbf{e}_\alpha$ be the contact force acting on the beam. Then equilibrium of forces acting on the wheel yields

$$\mathbf{F}_c = \mathbf{F} - M\ddot{\mathbf{y}} \,. \tag{3.13}$$

Thus, once the motion $\mathbf{y}$ of the wheel have been solved for, (3.13) can be used to compute the contact force. In the case of a moving magnet, the contact force $\mathbf{F}_c$ is the required active control force that should be exerted on the magnet to maintain a constant gap.

3.3. Small deformation assumptions. Equations (3.7) and (3.10) form the complete set of coupled, fully-nonlinear equations describing the motion of a rigid wheel moving over a flexible beam. In the present work, we limit our discussions to the case of structural equations which are linear in the displacement u^α. For this, the following assumptions are considered:

(A1) The structure deforms with small strains, and such that the spatial derivative of structural displacements is small: $|u^\alpha{}_{,S}| \ll 1$.

(A2) The Euler-Bernoulli hypothesis is assumed, with strain energy

$$\Psi(\mathbf{u}) = \frac{1}{2} \int_{[0,\, L]} \Big\{ EA\,[u^1{}_{,S}]^2 + \; EI\,[u^2{}_{,SS}]^2 \Big\} dS \,, \tag{3.14}$$

where EA is the axial stiffness and EI the bending stiffness.‡

‡ The frequencies in free vibration of a simply supported Euler-Bernoulli beam are accurate, compared with those of a Timoshenko beam, up to at least the 5th mode for a span/depth ratio greater than 20 (cf. Magrab [1979]).

(A3) In the inertia operator of the structural equations, only terms linear in the structural displacement u^α are retained; all nonlinear terms in u^α are neglected.

(A4) The wheel rolls without slipping and creeping. Structural deformation has negligible effects on its rotatory motion:

$$\theta(Y^1,t) \approx \frac{Y^1}{R}\,, \quad \frac{\partial\theta(Y^1,t)}{\partial S} \approx \frac{1}{R}\,, \quad \dot{\theta}(Y^1,t) \approx \frac{\dot{Y}^1}{R}\,, \quad \ddot{\theta}(Y^1,t) \approx \frac{\ddot{Y}^1}{R}\,.$$

In addition, we neglect the terms with factors $\frac{\partial\theta}{\partial u^\beta}$ and $\frac{\partial\theta}{\partial u^\beta{}_{,S}}$ in the structural equations of motion.

3.4. The mildly nonlinear equations of motion. Considering the structural equations of motion (3.10b), assumption (A3) implies that we neglect nonlinear terms in u^1 and u^2 in the fully-expanded expressions of $\ddot{g}^1$ and of $\ddot{g}^2$ obtained from using $(2.2)_1$ and (2.4b) in (3.11). Thus, together with assumption (A1), we arrive at the approximations

$$\ddot{g}^1 \approx \ddot{u}^1 - \bar{R}\ddot{u}^2{}_{,S}\,, \quad \ddot{g}^2 \approx \ddot{u}^2\,. \tag{3.15}$$

Note that approximations (3.15) together with relations (2.4) when applied to g^1 and g^2 imply

$$\frac{\partial^{i+j}g^1}{\partial S^i\partial t^j} \approx \frac{\partial^{i+j}u^1}{\partial S^i\partial t^j} - \bar{R}\frac{\partial^{i+j+1}u^2}{\partial S^{i+1}\partial t^j}\,, \quad \frac{\partial^{i+j}g^2}{\partial S^i\partial t^j} \approx \frac{\partial^{i+j}u^2}{\partial S^i\partial t^j}\,, \tag{3.16}$$

for $(i,j) = (1,0), (2,0), (1,1), (0,2)$. Further, assumptions (A1), (A3) and relation $(2.2)_1$ lead to the following approximations

$$\frac{\partial g^1}{\partial u^1{}_{,S}} \approx \bar{R}u^2{}_{,S}\,, \quad \frac{\partial g^1}{\partial u^2{}_{,S}} \approx -\bar{R}\,, \quad 1 + \frac{\partial g^1}{\partial S} \approx 1 - \bar{R}u^2{}_{,SS}\,, \tag{3.17a}$$

$$\frac{\partial g^2}{\partial u^1{}_{,S}} \approx 0\,, \quad \frac{\partial g^2}{\partial u^2{}_{,S}} \approx -\bar{R}u^2{}_{,S}\,, \quad \frac{\partial g^2}{\partial S} \approx u^2{}_{,S}\,. \tag{3.17b}$$

As a result of (2.4b), (3.15), (3.17), together with assumption (A4), the equation for the

nominal motion (3.7) can be approximated by

$$c_3(Y^1,t)\ddot{Y}^1 + c_2(Y^1,t)(\dot{Y}^1)^2 + c_1(Y^1,t)\dot{Y}^1 + c_o(Y^1,t) = 0\,, \tag{3.18a}$$

where

$$c_o(Y^1,t) \approx -F^1[1 - \bar{R}u^2{}_{,SS}(Y^1,t)] - F^2 u^2{}_{,S}(Y^1,t) - \frac{T}{R}$$

$$+ M\Big[[1 - \bar{R}u^2{}_{,SS}(Y^1,t)][u^1{}_{,tt}(Y^1,t) - \bar{R}u^2{}_{,Stt}(Y^1,t)] + u^2{}_{,S}(Y^1,t)u^2{}_{,tt}(Y^1,t)\Big]\,, \tag{3.18b}$$

$$c_1(Y^1,t) \approx 2M\Big[[1 - \bar{R}u^2{}_{,SS}(Y^1,t)][u^1{}_{,St}(Y^1,t) - \bar{R}u^2{}_{,SSt}(Y^1,t)] + u^2{}_{,S}(Y^1,t)u^2{}_{,St}(Y^1,t)\Big]\,, \tag{3.18c}$$

$$c_2(Y^1,t) \approx M\Big[[1 - \bar{R}u^2{}_{,SS}(Y^1,t)][u^1{}_{,SS}(Y^1,t) - \bar{R}u^2{}_{,SSS}(Y^1,t)] + u^2{}_{,S}(Y^1,t)u^2{}_{,SS}(Y^1,t)\Big]\,, \tag{3.18d}$$

$$c_3(Y^1,t) \approx M[1 - \bar{R}u^2{}_{,SS}(Y^1,t)]^2 + \frac{I_w}{R^2}\,. \tag{3.18e}$$

Remark 3.2. The nonlinear term in g^2 in the equation for the nominal motion (3.7) is, according to (3.15) and (3.17), approximated by

$$\frac{\partial g^2(Y^1,t)}{\partial S}\,\ddot{g}^2(Y^1,t) \approx u^2{}_{,S}(Y^1,t)\ddot{u}^2(Y^1,t)\,, \tag{3.19a}$$

which is also nonlinear in u^2. Using (2.4b) in (3.19a), we obtain the term (3.19a) in expanded form as given in (3.18). This term plays an important role in representing the influence of transverse structural displacement on vehicle nominal motion at high speed. To see this, we rewrite the equation for nominal motion (3.12a) of Maglev model C, for $F^1 = 0$, as follows

$$M\ddot{Y}^1 = u^2{}_{,S}(Y^1,t)\,[\,F^2 - M\ddot{u}^2(Y^1,t)\,] \equiv u^2{}_{,S}(Y^1,t)\,F_c^2(t)\,. \tag{3.19b}$$

At high speed, the vertical contact force F_c^2 may have a magnitude several times that of the vertical force F^2. We will present below examples where one has $|\,F_c^2(t)\,| > 1.5\,|\,F^2\,|$, for some time t, and for high-speed vehicle motion. In other words, the inertia force $M\ddot{u}^2$ can be of the same order of magnitude as that of F^2, and should be retained in equation (3.18). Hence, it is shown that the formulation would not

be appropriate for high speed regime, had we systematically removed all nonlinear terms in u^α from the equations of motion. This is at variance with the usual practice of complete linearization (see discussion in Kortüm [1986]), which is therefore inconsistent in the present situation. □

Next, using assumptions (A1-A4), the weak form of the equations for structural motion, linear in the displacement u^α, is given by

$$\eta^1(Y^1,t)\Big[-F^1 + M[\ddot{Y}^1 + \ddot{u}^1(Y^1,t) - \bar{R}\ddot{u}^2{}_{,S}(Y^1,t)]\Big] - \bar{R}[F^1 - M\ddot{Y}^1]\eta^1{}_{,S}(Y^1,t)u^2{}_{,S}(Y^1,t)$$

$$+ \int_{[0,\,L]} A_\rho \eta^1(S,t)u^1{}_{,tt}(S,t)dS + \int_{[0,\,L]} EA\,\eta^1{}_{,S}(S,t)u^1{}_{,S}(S,t)dS = 0\,, \tag{3.20a}$$

and

$$-\bar{R}\eta^2{}_{,S}(Y^1,t)\Big[-F^1 + M[\ddot{Y}^1 + \ddot{u}^1(Y^1,t) - \bar{R}\ddot{u}^2{}_{,S}(Y^1,t)]\Big]$$

$$+ \eta^2(Y^1,t)\Big[-F^2 + M\ddot{u}^2(Y^1,t)\Big] + \bar{R}F^2\eta^2{}_{,S}(Y^1,t)u^2{}_{,S}(Y^1,t)$$

$$\int_{[0,\,L]} A_\rho \eta^2(S,t)u^2{}_{,tt}(S,t)dS + \int_{[0,\,L]} EI\,\eta^2{}_{,SS}(S,t)u^2{}_{,SS}(S,t)dS = 0\,, \tag{3.20b}$$

for all admissible variations (η^1,η^2). It can be observed that the second term in (3.20a) and the third term in (3.20b) correspond to the geometric stiffness induced by the type of constraint considered in (3.11), and vanish for $\bar{R} = 0$. Next using (2.4), we could recast equations (3.20) in the following form

$$\Big[M\eta^1(Y^1,t)\Big(u^1{}_{,tt}(Y^1,t) - \bar{R}u^2{}_{,Stt}(Y^1,t)\Big) + \int_{[0,\,L]} A_\rho \eta^1(S,t)u^1{}_{,tt}(S,t)dS\Big]$$

$$+ 2M\dot{Y}^1\eta^1(Y^1,t)\Big[u^1{}_{,St}(Y^1,t) - \bar{R}u^2{}_{,SSt}(Y^1,t)\Big] + \Big[M\eta^1(Y^1,t)\Big(\ddot{Y}^1[u^1{}_{,S}(Y^1,t) - \bar{R}u^2{}_{,SS}(Y^1,t)]$$

$$+ (\dot{Y}^1)^2[u^1{}_{,SS}(Y^1,t) - \bar{R}u^2{}_{,SSS}(Y^1,t)]\Big) - \bar{R}[F^1 - M\ddot{Y}^1]\eta^1{}_{,S}(Y^1,t)u^2{}_{,S}(Y^1,t)$$

$$+ \int_{[0,\,L]} EA\,\eta^1{}_{,S}(S,t)u^1{}_{,S}(S,t)dS\Big] = \eta^1(Y^1,t)[F^1 - M\ddot{Y}^1]\,, \tag{3.21a}$$

and

$$\left[-\bar{R}M\eta^2{}_{,S}(Y^1,t)\left(u^1{}_{,tt}(Y^1,t)-\bar{R}u^2{}_{,Stt}(Y^1,t)\right)+ M\eta^2(Y^1,t)u^2{}_{,tt}(Y^1,t)+ \int_{[0,\,L]} A_\rho\eta^2(S,t)u^2{}_{,tt}(S,t)dS\right]$$

$$+ 2M\dot{Y}^1\left[-\bar{R}\eta^2{}_{,S}(Y^1,t)\left(u^1{}_{,St}(Y^1,t)-\bar{R}u^2{}_{,SSt}(Y^1,t)\right)+ \eta^2(Y^1,t)u^2{}_{,St}(Y^1,t)\right]$$

$$+ \left[M\ddot{Y}^1\left\{-\bar{R}\eta^2{}_{,S}(Y^1,t)\left(u^1{}_{,S}(Y^1,t)-\bar{R}u^2{}_{,SS}(Y^1,t)\right)+ \eta^2(Y^1,t)u^2{}_{,S}(Y^1,t)\right\}\right.$$

$$+ M(\dot{Y}^1)^2\left\{-\bar{R}\eta^2{}_{,S}(Y^1,t)\left(u^1{}_{,SS}(Y^1,t)-\bar{R}u^2{}_{,SSS}(Y^1,t)\right)+ \eta^2(Y^1,t)u^2{}_{,SS}(Y^1,t)\right\}$$

$$\left.+ \bar{R}F^2\eta^2{}_{,S}(Y^1,t)u^2{}_{,S}(Y^1,t)+ \int_{[0,\,L]} EI\eta^2{}_{,SS}(S,t)u^2{}_{,SS}(S,t)dS\right]$$

$$= -\bar{R}\eta^2{}_{,S}(Y^1,t)[F^1-M\ddot{Y}^1]+ \eta^2(Y^1,t)F^2\,, \tag{3.21b}$$

where terms are grouped in square brackets according to their nature (mass, velocity-convective, stiffness, and applied forces). Even though equations (3.18) and (3.21) are the simplified equations of motion of the system according to assumptions (A1) to (A4), they remain nonlinear and coupled. The above system of ODE/PDE's is driven by initial conditions $\{Y^1(0),\ \dot{Y}^1(0),\ \mathbf{u}(S,0),\ \mathbf{u}_{,t}(S,0)\}$ and the forces $\{F^1,\ F^2,\ T\}$ applied on the wheel. The algorithms discussed in the next section will allow one to integrate the complete system of equations of motion (3.18) and (3.21), without a-priori assumption of known nominal motion.

Remark 3.3. In relation to Remark 3.2, we note that the linearized structural equations of motion (3.20b) contains the (low order) effect of the contact force $F_c^2 = F^2 - M\ddot{u}^2$. Recall that, as pointed out in (3.19b), the contact force F_c^2 also appears in the equation for nominal motion (3.18). □

Remark 3.4. With assumptions (A1-A2) equation (3.12b) is decoupled into an equation of motion for axial vibration and an equation of motion for the transverse vibration. But then this means that the Maglev model C, unlike models A and B (see Remark 3.1), could not be used to study effects of vehicle accelerating or braking on the axial structural response. □

4. Numerical integration of equations of motion

In this section we describe numerical algorithms to solve the system of nonlinear, coupled equations of motion (3.18) and (3.21). Spatial discretization of these equations is discussed first. Then, two predictor/corrector algorithms, with a distinguished feature pertaining to our formulation, are proposed to solve in time the resulting semi-discrete equations of motion, which has the form of a system of DAE's. Finally, we introduce an expression for the discrete energy balance to later monitor the performance of the proposed algorithms.

4.1. Galerkin spatial discretization. For each $\alpha \in \{1,2\}$, let $\{P^{\alpha}_{Ii}(S);\ I = 1,...,N;\ i = 1,...,N^{\alpha}\}$, be a set of independent functions in S and satisfying the boundary conditions for u^{α}. We consider the following discretization

$$\eta^{\alpha}(S,t) \approx \sum_{I=1}^{N}\sum_{i=1}^{N^{\alpha}} P^{\alpha}_{Ii}(S)\eta^{\alpha}_{Ii}(t)\ , \quad u^{\alpha}(S,t) \approx \sum_{I=1}^{N}\sum_{i=1}^{N^{\alpha}} P^{\alpha}_{Ii}(S)d^{\alpha}_{Ii}(t)\ . \tag{4.1}$$

The functions $P^{\alpha}_{Ii}(S)$ may be eigenfunctions in the case of a simple structure and boundary conditions, or finite element interpolatory functions in the case of more complex structures. Introducing the discretization (4.1) into (3.18) and (3.21) we obtain a spatially-discrete system of equations of motion. Let $n := N^1 + N^2$; then the total number of structural degrees of freedom (dof's) of the discrete system is $\nu := Nn$.† Denoting $Z := \{Y^1,\ \dot{Y}^1\}^{\mathrm{T}}$, the equation for vehicle motion (3.18) could be recast into the first order form

$$\dot{Z} = \Phi(Z,\ \mathbf{d},\ t) := \left\{ \begin{array}{c} \dot{Y}^1 \\ \dfrac{-1}{c_3(Y^1,t)}[c_o(Y^1,t) + c_1(Y^1,t)\dot{Y}^1 + c_2(Y^1,t)(\dot{Y}^1)^2] \end{array} \right\}, \tag{4.2}$$

where the coefficients $c_i(Y^1,t)$ are computed according to (3.18) and using the approximation (4.1). We retain the second order form of the structural equations of motion,

† For a finite element discretization, n may be thought of as the number of dof's per node, and N the number of nodal point.

$$\mathbf{M}(Z)\ddot{\mathbf{d}} + \mathbf{V}(Z)\dot{\mathbf{d}} + \mathbf{S}(Z)\mathbf{d} = \mathbf{R}(Z,t)\,, \tag{4.3}$$

where $\mathbf{M}(Z) \in \mathbb{R}^{\nu\times\nu}$ is the mass matrix, $\mathbf{V}(Z) \in \mathbb{R}^{\nu\times\nu}$ the velocity-convective matrix, $\mathbf{S}(Z) \in \mathbb{R}^{\nu\times\nu}$ the stiffness matrix, $\mathbf{R}(Z,t) \in \mathbb{R}^{\nu\times 1}$ the applied force matrix, and $\mathbf{d}$ the column-matrix with components $d_{\text{II}}^{\alpha}(t)$. Note that to evaluate $\Phi = \{\Phi^1, \Phi^2\}^{\mathrm{T}}$ in (4.2), we need to know all values of $(\mathbf{d}, \dot{\mathbf{d}}, \ddot{\mathbf{d}})$. However, to alleviate the notation, only $\mathbf{d}$ appears in the argument list of Φ. Similarly, we do need $\overset{\bullet\bullet}{Y}{}^1$ in the evaluation of the stiffness $\mathbf{S}$ and the force $\mathbf{R}$ in (4.3), but only $Z = \{Y^1, \overset{\bullet}{Y}{}^1\}^{\mathrm{T}}$ would figure in their argument list.

Remark 4.1. In the case where finite element discretization is chosen, care should be taken in choosing interpolatory polynomials of sufficiently high order to ensure that spatial derivatives of u^α in (3.18) and (3.21) exist and are all represented. They should also be continuous across element boundaries — except when dictated by actual boundary conditions (see Examples 5.3 and 5.4). Recall that for relation (2.4b) to make sense, we need existence of spatial derivatives up to second order. Moreover, in the equations of motion, spatial derivatives are required up to second order for u^1 and third order for u^2. Enforced continuity of these higher derivatives makes the semi-discrete system (4.2) and (4.3) well-posed, and contributes to the good behavior in numerical results. Following traditional use in analysis of (Euler-Bernoulli) beam structures, several authors (e.g., Venancio-Filho [1978], Wallrapp [1986]) employ cubic Hermitian polynomials to interpolate the transverse displacement u^2 which have continuity only up to first order spatial derivative (i.e., $u^2{}_{,S}$). Moreover, if linear interpolatory function is used to approximate the axial displacement u^1, then terms in $u^1{}_{,SS}$ are artificially eliminated from the system. We note here that these discontinuities will not disappear by having more elements in the mesh, but appear on the other hand at a higher cadence. When passing over a discontinuity, often an algorithm with low order accuracy is used, unless the time step falls exactly on the discontinuity. An example of dropping in order of accuracy in the computed results due to discontinuity can be found in Deuflhard [1985]. □

The structure of the above matrices could easily be written in explicit form upon introducing the following definitions

$$\left\{\begin{matrix}\eta^1(S,t)\\ \eta^2(S,t)\end{matrix}\right\} \approx \sum_{I=1}^{N} \mathbf{P}_I^o(S)\eta_I(t)\,, \quad \left\{\begin{matrix}u^1(S,t)\\ u^2(S,t)\end{matrix}\right\} \approx \sum_{I=1}^{N} \mathbf{P}_I^o(S)\mathbf{d}_I(t)\,, \tag{4.4a}$$

$$\text{where} \quad \mathbf{P}_I^o(S) := \begin{bmatrix} \mathbf{Q}_I^1(S) & \mathbf{O}^{1\times N^2} \\ \mathbf{O}^{1\times N^1} & \mathbf{Q}_I^2(S) \end{bmatrix} \in \mathbb{R}^{2\times n}\,, \tag{4.4b}$$

$$\mathbf{Q}_I^\alpha(S) := \{P_{I1}^\alpha(S), \ldots, P_{IN^\alpha}^\alpha(S)\} \in \mathbb{R}^{1\times N^\alpha}\,, \tag{4.4c}$$

$$\eta_I(t) := \{\eta_{I1}^1, \ldots, \eta_{IN^1}^1, \eta_{I1}^2, \ldots, \eta_{IN^2}^2\}^{\mathrm{T}} \in \mathbb{R}^{n\times 1}\,, \tag{4.4d}$$

$$\mathbf{d}_I(t) := \{d_{I1}^1, \ldots, d_{IN^1}^1, d_{I1}^2, \ldots, d_{IN^2}^2\}^{\mathrm{T}} \in \mathbb{R}^{n\times 1}\,, \tag{4.4e}$$

with $\mathbf{O}^{i\times j}$ being the zero matrix in $\mathbb{R}^{i\times j}$. The displacement dof's of the beam can be ordered in $\mathbf{d}$ as follows

$$\mathbf{d}(t) = \{\mathbf{d}_1(t)^{\mathrm{T}} \,|\, \cdots \,|\, \mathbf{d}_N(t)^{\mathrm{T}}\}^{\mathrm{T}} \in \mathbb{R}^{\nu\times 1}\,. \tag{4.5}$$

Further, we define the following matrices,

$$\mathbf{P}_I^1(S) := \begin{bmatrix} \mathbf{Q}_I^1(S) & -\overline{R}\,\mathbf{Q}_{I,S}^2(S) \\ \mathbf{O}^{1\times N^1} & \mathbf{Q}_I^2(S) \end{bmatrix} \in \mathbb{R}^{2\times n}\,, \tag{4.6a}$$

$$\mathbf{A}_{IJ}^1(Y^1) := [\mathbf{P}_I^1(Y^1)]^{\mathrm{T}}\mathbf{P}_{J,S}^1(Y^1) \in \mathbb{R}^{n\times n}\,, \quad \mathbf{A}_{IJ}^2(Y^1) := [\mathbf{P}_I^1(Y^1)]^{\mathrm{T}}\mathbf{P}_{J,SS}^1(Y^1) \in \mathbb{R}^{n\times n}\,, \tag{4.6b}$$

$$\mathbf{A}_{IJ}^3(Y^1) := \overline{R} \begin{bmatrix} \mathbf{O}^{N^1\times N^1} & (M\ddot{Y}^1 - F^1)[\mathbf{Q}_{I,S}^1(Y^1)]^{\mathrm{T}}\mathbf{Q}_{J,S}^2(Y^1) \\ \mathbf{O}^{N^2\times N^1} & F^2[\mathbf{Q}_{I,S}^2(Y^1)]^{\mathrm{T}}\mathbf{Q}_{J,S}^2(Y^1) \end{bmatrix} \in \mathbb{R}^{n\times n}\,, \tag{4.6c}$$

where the subscript ",S" (",SS") designates differentiation with respect to S once (twice).

The mass matrix $\mathbf{M}(Z)$ can be decomposed as the sum of a constant part denoted by $\mathbf{M}^o$ and a time-varying part denoted by $\mathbf{M}^1(Z)$. Let $\mathbf{M}_{IJ}(Z) \in \mathbb{R}^{n\times n}$, for I,J $\in \{1,...,N\}$, be the submatrix of $\mathbf{M}$ that couples the dof's in $\mathbf{d}_I$ to those in $\mathbf{d}_J$; similarly for $\mathbf{M}_{IJ}^o$ and $\mathbf{M}_{IJ}^1(Z)$. Then,

$$\mathbf{M}_{IJ}(Z) = \mathbf{M}_{IJ}^o + \mathbf{M}_{IJ}^1(Z) \in \mathbb{R}^{n\times n}\,. \tag{4.7a}$$

We obtain from (3.21), (4.4), and (4.6a),

$$\mathbf{M}^o_{IJ} := \int_{[0,\,L]} A_\rho [\mathbf{P}^o_I(S)]^T \mathbf{P}^o_J(S) dS \in \mathbb{R}^{n\times n} \ , \quad \mathbf{M}^1_{IJ}(Z) := M[\mathbf{P}^1_I(Y^1)]^T \mathbf{P}^1_J(Y^1) \in \mathbb{R}^{n\times n} \ . \tag{4.7b}$$

It should be noted here that the mass matrix is symmetric, i.e., $\mathbf{M}_{IJ} = \mathbf{M}_{JI}$. However, such is not the case for the velocity-convective matrix $\mathbf{V}$ and the stiffness matrix $\mathbf{S}$ as will be seen shortly. From (3.21) and using the definitions in (4.6), an expression for $\mathbf{V}(Z)$ can be readily obtained as

$$\mathbf{V}_{IJ}(Z) = 2M\dot{Y}^1 \mathbf{A}^1_{IJ}(Y^1) \in \mathbb{R}^{n\times n} \ . \tag{4.8}$$

Analogous to the mass matrix $\mathbf{M}(Z)$, the stiffness matrix $\mathbf{S}(Z)$ is split up into a constant part $\mathbf{S}^o$ and a time-varying part $\mathbf{S}^1(Z)$ whose expressions are given by

$$\mathbf{S}_{IJ}(Z) = \mathbf{S}^o_{IJ} + \mathbf{S}^1_{IJ}(Z) \in \mathbb{R}^{n\times n} \ , \tag{4.9a}$$

$$\mathbf{S}^o_{IJ} := \int_{[0,\,L]} \begin{bmatrix} EA\,[\mathbf{Q}^1_{I,S}(S)]^T \mathbf{Q}^1_{J,S}(S) & \mathbf{O}^{N^1\times N^2} \\ \mathbf{O}^{N^2\times N^1} & EI[\mathbf{Q}^2_{I,SS}(S)]^T \mathbf{Q}^2_{J,SS}(S) \end{bmatrix} dS \in \mathbb{R}^{n\times n} \ , \tag{4.9b}$$

$$\mathbf{S}^1_{IJ}(Z) := M\ddot{Y}^1 \mathbf{A}^1_{IJ}(Y^1) + M(\dot{Y}^1)^2 \mathbf{A}^2_{IJ}(Y^1) + \mathbf{A}^3_{IJ}(Y^1) \in \mathbb{R}^{n\times n} \ . \tag{4.9c}$$

The first two terms in (4.9c) are convective terms, whereas the last term, $\mathbf{A}^3_{IJ}(Y^1)$, expresses the geometric effect induced by the constraints (3.11). Finally, the applied force corresponding to the degrees of freedom in $\mathbf{d}_I$ is

$$\mathbf{R}_I(Z,t) = [\mathbf{P}^1_I(Y^1)]^T \begin{Bmatrix} F^1 - M\ddot{Y}^1 \\ F^2 \end{Bmatrix} \in \mathbb{R}^{n\times 1} \ . \tag{4.10}$$

Remark 4.2. The above matrices acquire a particular structure when Galerkin finite-element discretization is used: The time-varying matrices $\mathbf{M}^1(Z)$, $\mathbf{V}(Z)$, and $\mathbf{S}^1(Z)$ contain zero coefficients except in a small submatrix located on their diagonal; for a discretization of the type (4.4), this submatrix is of dimension $2n\times 2n$ if each finite element has 2 nodal points. As the wheel moves (say, in the direction of increasing node numbers), the time-varying submatrices charge down along the diagonal of the global matrices.§ The reason for this particular structure of the convective matrices is the local

§ In a particular case of the present formulation, where only a point mass is considered ($I_w = 0$ and $\mathbf{A}^3_{IJ}(Z) = 0$) to be in contact with the structure, and where nominal motion is prescribed, the element matrices corresponding to the loaded element are referred to as "structure/vehicle element" in Olsson [1985-86].

character of finite element basis functions (functions with compact support). Similar observation could be made regarding the applied force $\mathbf{R}(Z,t)$. However, if the functions $P_{\mathrm{II}}^{\alpha}(S)$, are eigenfunctions of a vibrating beam, then all of the above matrices are full — but possibly of smaller order. □

4.2. Predictor/corrector temporal discretization. We are now ready to introduce discretization in time to solve the system of differential/algebraic equations of motion (4.2) and (4.3). In the general setting where a complex vehicle model (multibody system) is involved, equations of motion for the vehicle can be transformed into first order ODE's as in (4.2) (Führer [1986]). The dimension of the state space of a complex vehicle model could be of the same order as the number of structural dof's. It is noted that our numerical treatment in this section, even though applied here to the basic model, extends to this general setting.

In many simulation programs for vehicle dynamics, a reduced-order model for the structure is obtained by projecting (4.3) onto a subspace of eigenvectors (see, e.g., Wallrapp [1986] in relation to the program MEDYNA.),† and implies a frequency cut-off in the structural response. This reduced-order model is then transformed into the form of first order ODE's;‡ the cost of transforming the large system (4.3) into first order form being prohibitively expensive. Choice of the subspace of eigenvectors must be made carefully to represent all relevant effects in the motion, which are often difficult to guess in advance. The reason of this caution rests on the fact that the choice of an eigen-subspace that contains the maximum information on the motion depends intimately on the applied forces, i.e., a systematic selection of low frequency modes may lead to a misrepresentation of the motion. Further, recall that the projected matrices lose their bandedness, and are fully populated. In this paper, we propose methods of integrating (4.2) and (4.3) which retain the efficiency of structural dynamics algorithms for solving

† These eigenvectors correspond to the eigenvalue problem $\mathbf{S}^{o}\mathbf{x} = \lambda\mathbf{M}^{o}\mathbf{x}$.

‡ Vehicle nominal motion is prescribed a-priori here.

the unreduced system (4.3).

In what follows, the subscript $k+\varsigma_i$ will be used to designate the discrete approximate of a quantity at time $t_{k+\varsigma_i} \equiv t_k + \varsigma_i h$, where $\varsigma_i \in [0, 1]$, and h denotes the current time step size. Thus, for a function $f(t)$, we write $f_{k+\varsigma_i} \approx f(t_{k+\varsigma_i})$. The approximate to the structural displacement defined in (4.5) is written as $\mathbf{d}_{k+\varsigma_i} \approx \mathbf{d}(t_{k+\varsigma_i})$. Similarly, structural velocity and acceleration at time $t_{k+\varsigma_i}$ are denoted by $\mathbf{v}_{k+\varsigma_i} \approx \dot{\mathbf{d}}(t_{k+\varsigma_i})$ and $\mathbf{a}_{k+\varsigma_i} \approx \ddot{\mathbf{d}}(t_{k+\varsigma_i})$, respectively. Further, all dof's corresponding to u^α are gathered in

$$\mathbf{d}^\alpha := \{d^\alpha_{11}, \ldots, d^\alpha_{1N^\alpha} \mid \cdots \mid d^\alpha_{N1}, \ldots, d^\alpha_{NN^\alpha}\}^{\mathrm{T}} \in \mathbb{R}^{(NN^\alpha)\times 1}, \tag{4.11a}$$

and thus

$$\mathbf{v}^\alpha_{k+\varsigma_i} \approx \dot{\mathbf{d}}^\alpha(t_{k+\varsigma_i}), \quad \mathbf{a}^\alpha_{k+\varsigma_i} \approx \ddot{\mathbf{d}}^\alpha(t_{k+\varsigma_i}). \tag{4.11b}$$

In addition, we introduce the following expressions for later use

$$\mathbf{K}(Z_{k+\varsigma_i}) := \left[\mathbf{M}(Z_{k+\varsigma_i}) + \varsigma_i h(\tfrac{3}{2}-\gamma)\mathbf{V}(Z_{k+\varsigma_i}) + \frac{\varsigma_i^2 h^2}{4\gamma^2}\mathbf{S}(Z_{k+\varsigma_i})\right] \in \mathbb{R}^{\nu\times\nu}, \tag{4.12a}$$

$$\begin{aligned}\mathbf{f}(Z_{k+\varsigma_i}, t_{k+\varsigma_i}) := {} & \mathbf{R}(Z_{k+\varsigma_i}, t_{k+\varsigma_i}) - \mathbf{V}(Z_{k+\varsigma_i})[\mathbf{v}_k + \varsigma_i h(2\gamma - \tfrac{3}{2})\mathbf{a}_k] \\ & - \mathbf{S}(Z_{k+\varsigma_i})\left[\mathbf{d}_k + \varsigma_i h\gamma\mathbf{v}_k + \frac{\varsigma_i^2 h^2}{2}\left(1 - \frac{1}{2\gamma^2}\right)\mathbf{a}_k\right] \in \mathbb{R}^{\nu\times 1},\end{aligned} \tag{4.12b}$$

$$\mathbf{v}_{k+\varsigma_i} = \mathbf{v}_k + \varsigma_i h\left[(\gamma - \tfrac{1}{2})\mathbf{a}_k + (\tfrac{3}{2}-\gamma)\mathbf{a}_{k+\varsigma_i}\right] \in \mathbb{R}^{\nu\times 1}, \tag{4.13a}$$

$$\mathbf{d}_{k+\varsigma_i} = \mathbf{d}_k + \varsigma_i h\mathbf{v}_k + \frac{\varsigma_i^2 h^2}{2}\left[\left(1 - \frac{1}{2\gamma^2}\right)\mathbf{a}_k + \frac{1}{2\gamma^2}\mathbf{a}_{k+\varsigma_i}\right] \in \mathbb{R}^{\nu\times 1}. \tag{4.13b}$$

The following algorithm is a single-step predictor/corrector that combines explicit methods of the Runge-Kutta family with an efficient algorithm in structural dynamics for solving (4.2) and (4.3).

Algorithm 1: (single-step predictor/corrector)

Data: • Algo. const.: γ, p, $\{\varsigma_i;\ i=1,\ldots,p\}$,
$\{a_{ij};\ i=2,\ldots,p,\ j=1,\ldots,(i-1)\}$, $\{b_i;\ i=1,\ldots,p\}$,

- Current time step size h,
- Solution at time t_k: Z_k, $\mathbf{d}_k$, $\mathbf{v}_k$, $\mathbf{a}_k$.

Predictor:

1) $D_1 = h\Phi(Z_k, \mathbf{d}_k, t_k)$.

For each $(i \in \{2,...,p\})$, **do** {

2) $\hat{Z}_{k+\varsigma_i} = Z_k + \sum_{j=1}^{i-1} a_{ij} D_j$.

3) Solve for $\hat{\mathbf{a}}_{k+\varsigma_i}$ such that $\mathbf{K}(\hat{Z}_{k+\varsigma_i})\, \hat{\mathbf{a}}_{k+\varsigma_i} = \mathbf{f}(\hat{Z}_{k+\varsigma_i}, t_{k+\varsigma_i})$, where $\mathbf{K}$ and $\mathbf{f}$ are computed as in (4.12).

4) *Displacement*: Compute $\hat{\mathbf{d}}_{k+\varsigma_i}$ using $\hat{\mathbf{a}}_{k+\varsigma_i}$ as in (4.13b).

5) *Axial velocity*: Set $\hat{\mathbf{v}}^1_{k+\varsigma_i} \equiv \mathbf{v}^1_k$,
Transverse velocity: Compute $\hat{\mathbf{v}}^2_{k+\varsigma_i}$ using $\hat{\mathbf{a}}^2_{k+\varsigma_i}$ as in (4.13a).

6) *Axial acceleration*: Set $\hat{\mathbf{a}}^1_{k+\varsigma_i} \equiv 0$.

7) $D_i = h\Phi(\hat{Z}_{k+\varsigma_i}, \hat{\mathbf{d}}_{k+\varsigma_i}, t_{k+\varsigma_i})$.

}

Corrector:

8) $Z_{k+1} = Z_k + \sum_{i=1}^{p} b_i D_i$.

9) Solve for $\mathbf{a}_{k+1}$ such that $\mathbf{K}(Z_{k+1})\, \mathbf{a}_{k+1} = \mathbf{f}(Z_{k+1}, t_{k+1})$, where $\mathbf{K}$ and $\mathbf{f}$ are computed as in (4.12).

10) Compute $\mathbf{v}_{k+1}$ and $\mathbf{d}_{k+1}$ using $\mathbf{a}_{k+1}$ as in (4.13).

□

Remark 4.3. Assuming that the structural displacement $\mathbf{d}(t)$ is known exactly for all $t \in [0,+\infty)$ then with $\mathbf{d}_k \equiv \mathbf{d}(t_k)$, $\forall\ k$, Steps 1,2,7 and 8 in Algorithm **1** constitute the explicit p-stage Runge-Kutta method, with coefficients ς_i, a_{ij} and b_i, and solving for $Z(t)$. Recall that for the 4-stage classical Runge-Kutta method (4th-order accurate), we have $\{\varsigma_i\} = \{0, \frac{1}{2}, \frac{1}{2}, 1\}$, $a_{ij} = 0$ except $\{a_{21}, a_{32}, a_{43}\} = \{\frac{1}{2}, \frac{1}{2}, 1\}$, and $\{b_i\} = \{\frac{1}{6}, \frac{1}{3}, \frac{1}{3}, \frac{1}{6}\}$ (see, e.g., Butcher [1987]).† Instead of the first order form (4.2) it would be advantageous, in the present basic problem, to consider directly the second order form of the equation for nominal motion, i.e., $\ddot{Y}^1 = \Phi^2(Y^1, \dot{Y}^1, \mathbf{d}, t)$, and employ instead the Runge-Kutta-Nyström algorithm (Bettis [1973], Dormand & Prince [1978]). However,

† A *convention* often valid for almost all Runge-Kutta schemes is: $\varsigma_i = \sum_{j=1}^{p} a_{ij}$ (Dekker & Verwer [1984]).

Führer [1986] points out that for a general vehicle model the first order ODE form of the vehicle equations of motion is still de rigueur (see Führer & Wallrapp [1984] and Nikravesh [1984] for methods of transforming DAE's of vehicle systems into ODE's by elimination of algebraic constraints). □

Remark 4.4. If the nominal motion $Y^1(t)$ (or $Z(t)$) is known a-priori, then with $Z_{k+1} \equiv Z(t_{k+1})$, $\forall\ k$, Steps 9 and 10 in Algorithm **1** express balance of momentum at time t_{k+1}, and correspond to the implicit "θ_1-method" proposed by Hoff [1986]. We note that to derive (4.12a-b) from the balance of momentum (4.3) at time $t_{k+\varsigma_i}$, the following relations are used

$$\mathbf{v}_{k+\varsigma_i} = \mathbf{v}_k + \varsigma_i h\left[(2\gamma - \tfrac{3}{2})\mathbf{a}_k + (\tfrac{3}{2} - \gamma)\mathbf{a}_{k+\varsigma_i}\right] \in \mathbb{R}^{\nu\times 1}\,, \tag{4.14a}$$

$$\mathbf{d}_{k+\varsigma_i} = \mathbf{d}_k + \varsigma_i h\gamma\mathbf{v}_k + \frac{\varsigma_i^2 h^2}{2}\left[\left(1 - \frac{1}{2\gamma^2}\right)\mathbf{a}_k + \frac{1}{2\gamma^2}\,\mathbf{a}_{k+\varsigma_i}\right] \in \mathbb{R}^{\nu\times 1}\,. \tag{4.14b}$$

These relations are slightly different than (4.13a-b), and effectively introduce numerical dissipation in the high frequencies (for $\gamma \neq 1$). This algorithm is unconditionally stable for $\gamma \in [0.5, 1]$, and is (locally) second order accurate. However, in order to have no overshooting, small algorithmic damping, and small relative period error, it is recommended to use $\gamma \in [0.95, 1]$ (Hoff & Pahl [1987]). For $\gamma = 1$, the method reduces to the trapezoidal rule with well understood properties (see, e.g., Hughes [1983]). We note that displacement or velocity, instead of acceleration as presented in Steps 3 and 9, could be equivalently chosen as primary unknown. The "θ_1-method" is close to the trapezoidal rule in the low frequency range, and offers numerical dissipation in the high frequency range — this type of method could be employed if such "low-pass filtering" effect is desired. Recall on the other hand that the trapezoidal rule is free of numerical dissipation in the whole frequency range, and is thus able to reflect with fidelity properties of the spatial discretization. □

The "θ_1-method" (implicit, unconditionally stable) is employed to predict structural response for the intermediate steps of the Runge-Kutta scheme (explicit, conditionally stable) with a special treatment for axial motion: In the computation of D_i, for $i=2,...,p$, the axial velocity $\hat{\mathbf{v}}^1_{k+\varsigma_i}$ is reset to its value at time t_k (see Step 5), while the axial acceleration $\hat{\mathbf{a}}^1_{k+\varsigma_i}$ is reset to zero (see Step 6). In fact, instead of Steps 5 and 6, we could have retained the axial acceleration as computed in Step 3, and evaluate the axial velocity according to (4.13a). However, this treatment is found to effectively maintain stability of the numerical algorithm by preventing high oscillations with unbounded growth of energy, as will be demonstrated in numerical examples below. Explanation of the mechanism triggering this growth in energy is deferred until later in the examples section.

We mention in passing that for systems with constant coefficients, the "θ_1-method" shares similar properties with the "α-method" proposed by Hilber, Hughes & Taylor [1977]. The former possesses some advantages over the latter, but more importantly, lends itself nicely to nonlinear systems with time-varying coefficients. Other type of single-step structural dynamics algorithms, such as the "beta-m" method by Katona & Zienkiewicz [1985], could also be employed. However, explicit integration methods, even with high order of accuracy, are not recommended for this problem because of their severe restriction on the time step size (conditional stability). An unconditionally stable "explicit" algorithm was proposed by Trujillo [1972],‡ but suffers poor accuracy (Belytschko [1983]). Further, a foremost advantage of explicit methods over implicit methods rests on the constancy of the mass matrix (or better yet, a diagonal mass matrix). This advantage is quickly nullified if the mass matrix is non-diagonal, and has time-dependent coefficients such as in the present study. A recent state-of-the-art review by Wood [1987] provides an extensive survey into numerical integrators employed in

‡ This method is based on application of operator splitting to the trapezoidal rule to avoid solving a system of linear equations.

structural dynamics. A word of caution is here warranted: Since most of the above-mentioned algorithms were analyzed for a scalar differential equation (except the algorithm by Gellert [1978]) with constant coefficients, their properties should not be freely extended to systems with time-varying coefficients and with non-modal "damping" as that encountered in the present study. As a consequence, the trapezoidal rule is definitely adequate in our case.

In Algorithm **1**, each step i (except Step 1) in the predictor stage requires solving a system of linear equations to predict the structural motion. This process, often referred to as function evaluation, is particularly an expensive step in our problem. Linear multistep methods require less function evaluations than single-step Runge-Kutta methods, and therefore will prove to be advantageous in decreasing computational effort in the present study.† We consider therefore in Algorithm **2** a combination of linear multistep methods and the "θ_1-method." Let

$$\Phi_k^{[i]} := \Phi^{[i]}(Z_k,\, \mathbf{d}_k,\, t_k)\,, \quad \text{where} \quad \Phi^{[i]} := \frac{d^{i+1}Z}{dt^{i+1}}\,, \quad \text{and} \quad \Phi^{[0]} \equiv \Phi\,. \tag{4.15}$$

Algorithm 2: (linear multistep predictor/corrector)

Data:
- Algo. const.: $\gamma,\ q,\ m,\ \{\alpha_i,\, \beta_i;\ i=1,...,q\},\ \{\lambda_i,\, \mu_i;\ i=0,...,(q-1)\}$,
- Current time step size h,
- Solution at time t_k: $\{Z_k,\, \Phi_k^{[0]},\, \ldots,\, \Phi_k^{[q]}\},\ \mathbf{d}_k,\ \mathbf{v}_k,\ \mathbf{a}_k$.

Predictor (P):

1) Compute $\{\Phi_{k-1},\, \ldots,\, \Phi_{k-q+1}\}$ from $\{\Phi_k^{[0]},\, \ldots,\, \Phi_k^{[q]}\}$.
2) $Z_{k+1}^{(0)} = \sum_{j=1}^{q} [\alpha_j Z_{k-j+1} + h\beta_j \Phi_{k-j+1}]$.
3) Solve for $\mathbf{a}_{k+1}^{(0)}$ such that $\mathbf{K}(Z_{k+1}^{(0)})\, \mathbf{a}_{k+1}^{(0)} = \mathbf{f}(Z_{k+1}^{(0)},\, t_{k+1})$, where $\mathbf{K}$ and $\mathbf{f}$ are computed as in (4.12).
4) *Displacement*: Compute $\mathbf{d}_{k+1}^{(0)}$ using $\mathbf{a}_{k+1}^{(0)}$ as in (4.13b).
5) *Axial velocity*: Set $\left(\mathbf{v}_{k+1}^1\right)^{(0)} \equiv \mathbf{v}_k^1$,
   Transverse velocity: Compute $\left(\mathbf{v}_{k+1}^2\right)^{(0)}$ using $\left(\mathbf{a}_{k+1}^2\right)^{(0)}$ as in (4.13a).

† In general, when solving ODE's, one should also account for the overhead cost. Then linear multistep methods do not necessarily come out as winners over Runge-Kutta methods (Gupta [1980]).

6) *Axial acceleration*: Set $\left(\mathbf{a}_{k+1}^{1}\right)^{(0)} \equiv 0$.

Corrector $(\mathrm{EC})^m$:

For each $(i \in \{1,\ldots,m\})$, **do** {

7) Evaluate $\Phi_{k+1} = \Phi(Z_{k+1}^{(i-1)}, \mathbf{d}_{k+1}^{(i-1)}, t_{k+1})$.

8) $Z_{k+1}^{(i)} = \sum_{j=0}^{q-1} [\lambda_j Z_{k-j} + h\mu_j \Phi_{k-j+1}]$.

9) Solve for $\mathbf{a}_{k+1}^{(i)}$ such that $\mathbf{K}(Z_{k+1}^{(i)})\, \mathbf{a}_{k+1}^{(i)} = \mathbf{f}_k(Z_{k+1}^{(i)}, t_{k+1})$, where $\mathbf{K}$ and $\mathbf{f}_k$ are computed as in (4.12).

10) Compute $\mathbf{v}_{k+1}^{(i)}$ and $\mathbf{d}_{k+1}^{(i)}$ using $\mathbf{a}_{n+1}^{(i)}$ as in (4.13).

}

11) *Evaluation* (E): $\Phi_{k+1} = \Phi(Z_{k+1}^{(m)}, \mathbf{d}_{k+1}^{(m)}, t_{k+1})$.

□

Remark 4.5. In the above, Step 2 contains the q-step Adams-Bashford and the Crane-Klopfenstein methods, whereas Step 5 may be specialized to the $(q-1)$-step Adams-Moulton method, with m being the number of simple iterations in the corrector stage (see, e.g., Lambert [1973]). For $q = 4$, the 4-step Adams-Bashford method has coefficients

$$\alpha_1 = 1\ , \quad \alpha_2 = \alpha_3 = \alpha_4 = 0\ , \quad \text{and} \quad \{24\beta_i\} = \{55, -59, 37, -9\}\ ,$$

while the Crane-Klopfenstein method has coefficients

$\alpha_1 = \quad 1.547652$	$\beta_1 = \quad 2.002247$
$\alpha_2 = -1.867503$	$\beta_2 = -2.031690$
$\alpha_3 = \quad 2.017204$	$\beta_3 = \quad 1.818609$
$\alpha_4 = -0.697353$	$\beta_4 = -0.714320$

and the 3-step Adams-Moulton method has coefficients

$$\lambda_0 = 1\ , \quad \lambda_1 = \lambda_2 = \lambda_3 = 0\ , \quad \text{and} \quad \{24\mu_i\} = \{9, 19, -5, 1\}\ . \quad \square$$

Remark 4.6. In step 1, with the step size h given, the value of $\{\Phi_{k-1}, \ldots, \Phi_{k-q+1}\}$ from $\{\Phi_k^{[0]}, \ldots, \Phi_k^{[q]}\}$ (and vice versa) is easily obtained by interpolation of a polynomial of degree q (see, e.g., Gear [1971, p.149]). This procedure (due to Nordsieck) allows a convenient change of time step size. □

Algorithm **2** is a general predictor/corrector in $P(EC)^m E$ mode. For $m = 1$ and $q = 4$, the Crane-Klopfenstein predictor combined with the 3-step Adams-Moulton corrector is of 4th-order, and has a region of absolute stability comparable to that of the classical (4th-order) Runge-Kutta method. This region of absolute stability is more than twice larger than that of the Adams-Bashford-Moulton method in both $P(EC)^2$ mode and in *PECE* mode (Lambert [1973, p.148]). Even though the two Algorithms **1** and **2** have similar properties regarding accuracy and stability, the computational effort in Algorithm **2** with *PECE* mode is twice less: It requires only two solutions for structural motion, instead of four as in Algorithm **1**. Therefore, Algorithm **2** is definitely more efficient than Algorithm **1**, except that it is not self-starting. We will use Algorithm **1** to create the starting points for Algorithm **2**.

Even though more efficient starters based on methods proposed by Gear [1980] could be developed, but considering that the overall saving is not significant, in the present work, all results are reported with Algorithm **1** as starter for Algorithm **2**. Robustness of the proposed predictor/corrector algorithms rests in part on the unconditional stability of the "θ_1-method." Methods other than linear multistep ones, such as extrapolation methods, could be explored as alternatives (Gupta, Sacks-Davis & Tischer [1985]). Deuflhard [1985] provides an extensive review of extrapolation methods. Finally, we note that the proposed algorithms are extendible to the case with fully nonlinear beam theory (see Vu-Quoc [1986] and Vu-Quoc & Simo [1987] for a related algorithm to solve an ODE/PDE system arised in satellite dynamics).

4.3. Discrete energy balance. The balance of system energy at time t can be written as follows

$$\mathbb{K}_t + \Psi_t - \int_0^t [\, F^\alpha(\tau)\dot{y}^\alpha(\tau) + T(\tau)\dot{\theta}(\tau)\,]\, d\tau = \mathbb{K}_o + \Psi_o\,, \tag{4.16}$$

where $\mathbb{K}_t$ and Ψ_t are as given respectively in (2.3) and (3.14), the integral term is the work done by external forces, $\mathbb{K}_o$ the initial kinetic energy, and Ψ_o the initial potential

energy. For small structural deformations, we consider the following approximation to the kinetic energy and potential energy

$$K_t \approx \frac{1}{2} M\left\{[\dot{Y}^1 + \dot{u}^1(Y^1,t) - \bar{R}\dot{u}^2{}_{,S}(Y^1,t)]^2 + [\dot{u}^2(Y^1,t)]^2\right\} + \frac{1}{2} I_w \left(\frac{\dot{Y}^1}{R}\right)^2 + \frac{1}{2} \dot{\mathbf{d}}^{\mathrm{T}} \mathbf{M}^e \dot{\mathbf{d}}\,, \quad (4.17a)$$

$$\Psi_t \approx \frac{1}{2} \mathbf{d}^{\mathrm{T}} \mathbf{S}^e \mathbf{d}\,, \quad (4.17b)$$

where $\dot{u}^\alpha$ is to be interpreted in the sense of (2.4a). It is important to note that despite the approximation to the velocity employed in (4.17a), the equations of motion (3.18) and (3.20) remain an approximation to the Euler-Lagrange equations derived from using this approximated kinetic energy in the Lagrangian (3.1). However, for small deformations, this is a good approximation. The energy balance (4.16) together with approximations (4.17) provide a very useful guideline in the design of numerical integration methods. We will show by numerical examples that the proposed algorithms maintain well energy balance to within very small error tolerance. Recall that in linear structural dynamics, the trapezoidal rule preserves exactly system energy (e.g., Hughes [1983]). In addition to providing an indication to the soundness of integration algorithms, energy balance is used to explain the Timoshenko paradox mentioned in the introduction.

5. Numerical examples

In this section, numerical results for our basic model of vehicle/structure interaction are presented for a wide range of vehicle speeds. Emphasis is focused on results which are not achievable using formulations based on the traditional assumption of known vehicle nominal motion. Further, these examples demonstrate the adequacy of the present formulation for vehicles moving at high speed on flexible structures, as well as the reliability and efficiency of the proposed integration algorithms.

Finite element basis functions are used here in the discretization (4.4) such that for a partition $0 \equiv S_1 < \ldots < S_N \equiv L$, the dof's associated with node $\mathrm{I} \in \{1,\ldots,N\}$ are the displacement components and their spatial derivatives (see (4.4e)):

$$d_{\mathrm{I}i}^{\alpha} \approx \frac{\partial^{i-1} u^{\alpha}(S_{\mathrm{I}}, t)}{\partial S^{i-1}} \,. \tag{5.1}$$

For complete continuity of the spatial derivatives appearing in (3.18) and (3.21), one should use (at least) $N^1 = 3$ for the axial dof's, and $N^2 = 4$ for the transverse dof's. There are thus seven dof's at each nodal point. It is easy to construct the basis functions $P_{\mathrm{I}i}^{\alpha}$ corresponding to these dof's in terms of polynomials: For the axial displacement, $P_{\mathrm{I}i}^{1}$ is a 5th-order polynomial, while for the transverse displacement $P_{\mathrm{I}i}^{2}$ is a 7th-order polynomial.

The proposed numerical procedure for analyzing vehicle/structure interaction has been implemented in the research version of FEAP, the Finite Element Analysis Program developed by R.L. Taylor — see Zienkiewicz [1977, Chap. 24] for a description of a simple version. The beam element used in our work is implemented to allow the flexibility to choose different number of nodal dof's, i.e., different values of N^1 and N^2.

All numerical results reported herein are obtained with the following algorithm constants. In Algorithm **1**, we use the constants for the classical Runge-Kutta method (Remark 4.3), and in Algorithm **2** the constants for the Crane-Klopfenstein and the Adams-Moulton methods (Remark 4.5). The *PECE* mode is chosen for Algorithm **2** ($m = 1$), and Algorithm **1** is used to compute the starting points. Integration of structural motion is performed with $\gamma = 1$, i.e., the trapezoidal rule. In all examples, the time step size is kept constant throughout the calculation. Effects of vehicle/structure interaction will be studied in the following examples for a simple-span and a six-span beam structure depicted in Figure 5.0. Also, all beam structures and their spatial discretizations are uniform.

Example 5.1. Vehicle/structure interaction at different initial velocities. Consider a wheel of mass $M = 3000kg$, rotatory inertia $I_w = 135kgm^2$, radius $R = 0.3m$, rolling over a simply supported beam. The distance from the beam centroidal line to the wheel center of mass is $\overline{R} = 0.9m$. The beam has a length $L = 24m$, mass per unit

length $A_\rho = 1250kg/m$, axial stiffness $EA = 5\times 10^9 N$, and bending stiffness $EI = 10^9 Nm^2$. The wheel is subjected to a constant vertical force $F^2 = -600{,}000N$ (cf. Figure 5.0). The magnitude of this force is about 20 times that of the weight of the wheel (acceleration of gravity $9.81m/s^2$). The maximum mid-span static deflection corresponding to this load is $0.1728m$ or about $L/140$.

The lowest flexural frequency is $2.44Hz$; the lowest axial frequency is $20.8Hz$ (see Remark 5.1). The following initial conditions are considered: $Y^1(0) = 0$, $\mathbf{u}(S,0) = \mathbf{u}_{,t}(S,0) \equiv 0$. The wheel motion is driven mainly by its initial velocity $\dot{Y}^1(0)$. Four values of initial velocities — $1m/s$, $10m/s$, $50m/s$, and $100m/s$ — are chosen to study the effects of complete vehicle/structure interaction. Often, the non-dimensional quantity

$$\alpha = \frac{\dot{Y}^1}{2\, f_1^2\, L}, \tag{5.2}$$

where f_1^2 is the lowest flexural frequency of a beam of length L, is used to describe the dynamic character of moving load problems (see Frýba [1972]). In this example, the above initial velocities correspond to the values of α of 0.00854, 0.0854, 0.427, and 0.854, respectively. To integrate the motion, we used 200 time steps with respect to the traversing time on a rigid beam for each of the four cases (i.e., $24s$, $2.4s$, $0.48s$, and $0.24s$). Thus, the time step size h takes respectively the values $0.12s$, $0.012s$, $0.0024s$, and $0.0012s$.

Nominal velocity. Time histories of nominal velocity for different initial velocities are plotted in Figures 5.1a-d. The largest increase in nominal velocity (about 400%) is obtained for the smallest initial velocity ($\dot{Y}^1(0) = 1m/s$, Figure 5.1a). As a result, the traversing time on the present flexible beam is about one third of the traversing time on a rigid beam. For an initial velocity of $10m/s$, the increase in velocity is drastically reduced to about 10% (Figure 5.1b), with an exit velocity of $9.96m/s$. From Figures 5.1c-d, one can clearly observe a loss in nominal velocity at the end of the traversing: An initial velocity of $50m/s$ drops by 1.2% to an exit velocity of $49.4m/s$, while an initial

velocity of $100m/s$ drops by 0.7% to an exit velocity of $99.34m/s$. The peak-to-peak variations in nominal velocity for these two cases are respectively 1.7% and 1.0% of the initial velocity. For $\dot{Y}^1(0) = 100m/s$, an analysis with 100 time steps, i.e., with $h = 0.0024s$, shows little difference in the results (Figure 5.1d). We will therefore use this time step size in the case of a six-span beam below (Examples 5.3 and 5.4).

Structural deflection. The greater loss of velocity for $\dot{Y}^1(0) = 50m/s$ is due to the larger vertical displacement at the contact point, as recorded in Figure 5.1e. We note the shift of the location of maximum displacement closer to the exit as initial velocity increases. Figure 5.1f shows the vertical mid-span displacement for different initial velocities, where time is normalized with respect to the traversing time on a rigid beam for each case. The dynamic magnification factor is 1.61 for $\dot{Y}^1(0) = 50m/s$, and 1.77 for $\dot{Y}^1(0) = 100m/s$. Observe the free vibration of the beam, after the traversing of the vehicle, clearly shown for $\dot{Y}^1(0) = 1m/s$.

Contact force. Recorded in Figure 5.1g are time histories of the vertical contact force F_c^2, for initial velocities of $50m/s$ and $100m/s$. As noted in Remark 3.2, the inertia force $M\ddot{u}^2$ is non-negligible at high speed, as attested by the magnitude of the normalized contact force in Figure 5.1g: For an initial velocity of $100m/s$, this inertia force could reach 60% of the vertical force F^2. The vertical contact force F_c^2 and the vertical force F^2 differ only slightly at low speed — for the initial velocities of $1m/s$ and $10m/s$, this difference is computed to be within 3% of the vertical force F^2.

Energy balance. The soundness of numerical algorithms depends in part on how well the computed results satisfy energy balance. The variation of the terms in the expression for energy balance (4.16), as a function of time, for an initial velocity of $10m/s$ is plotted in Figure 5.1h, where the legend "energy balance" means the left hand side of (4.16). (At this scale, the kinetic energy of the beam is too small to be well discernible, and is not plotted.)

Using Algorithm **1** throughout, the maximum offset of energy balance for $\dot{Y}^1(0) = 10m/s$ is 0.13% of the initial kinetic energy $I\!K_o$ ($= 0.225\times 10^6 kgm^2/s^2$); this maximum offset is about 0.03% of $I\!K_o$ ($= 5.625\times 10^6 kgm^2/s^2$) for $\dot{Y}^1(0) = 50m/s$, and 0.018% of $I\!K_o$ ($= 22.5\times 10^6 kgm^2/s^2$) for $\dot{Y}^1(0) = 100m/s$.

Using Algorithm **2**, with Algorithm **1** as starter, the offset of energy balance for $\dot{Y}^1(0) = 10m/s$ is 0.27% of $I\!K_o$. The maximum offset occurs at the transition from Algorithm **1** to Algorithm **2** at the start of the calculation, as shown in Figure 5.1i. From then on, both curves in this figure show a similar pattern. A smaller time step size should be used to reduce this initial offset. On the other hand, the maximum offset in energy balance for initial velocities of 50 and $100m/s$ are 0.014% and 0.008% of their respective $I\!K_o$. These maxima occur near the end of the traversing. Thus, the offset of energy balance in Algorithm **2** is roughly half of that produced in Algorithm **1**. This remark is also true in later examples. Algorithm **2** therefore not only reduces significantly the computational effort, but satisfies better the energy balance in comparison with Algorithm **1**.

Plotted in Figure 5.1j are both the energy balance and the wheel kinetic energy as a function of time for $\dot{Y}^1(0) = 100m/s$. The drop in nominal velocity at the exit (Figure 5.1d) induces a loss in the vehicle kinetic energy, as part of this energy is transferred to the beam to leave the beam in free vibration after the passage of the vehicle. This energy transfer effectively explains the Timoshenko paradox. One would then immediately ask how much the drop in nominal velocity would be for a vehicle moving over a multiple-span beam structure. This situation will be considered in Example 5.3.

Remark 5.1. For completeness, we record here the computed eigen-frequencies of the above simply supported beam using different types of spatial discretization. Let f_i^{α} be the frequency of the *ith* mode for displacement u^{α}. Expressions for of the exact frequencies are

$$f_i^1 = \frac{(2i-1)}{4L}\left(\frac{EA}{A_\rho}\right)^{\frac{1}{2}}, \quad f_i^2 = \frac{i^2\pi}{2L^2}\left(\frac{EI}{A_\rho}\right)^{\frac{1}{2}}. \tag{5.3}$$

Refinement (h-version or p-version) of spatial discretization is characterized by the triplet (N, N^1, N^2). We recall that N is the number of nodal points, and N^α is the number of dof's per node corresponding to displacement u^α. Reported in the third column of Table 5.1 are the frequencies obtained with the discretization of type (3,3,4), which was used in the above calculation. The beam thus has 7 dof's for axial displacement u^1, and 8 dof's for transverse displacement u^2 (boundary conditions included).

Table 5.1. *Eigen-frequencies of simply supported beam.*

Frequency	Exact	Computed with Discretization (N,N^1,N^2)			
(Hz)	values	(3,3,4)	(3,1,2)	(8,1,0)	(5,0,2)
f_1^1	20.8333	20.8333	21.3721	20.8771	—
f_2^1	62.5000	62.5000	74.6610	63.6859	—
f_1^2	2.43917	2.43917	2.44880	—	2.43981
f_2^2	9.75669	9.75669	10.8291	—	9.79520
f_3^2	21.9525	21.9530	27.2199	—	22.3537
f_4^2	39.0267	39.0279	49.6253	—	43.3165
f_5^2	60.9793	61.3685	—	—	68.8514

For a fair comparison of performance with the lower order p-discretization (N^1, N^2) = (1,2), we consider in the last three columns: (i) discretization (3,1,2) which has 3 nodes, (ii) discretization (8,1,0) which has 7 axial dof's, and (iii) discretization (5,0,2) which has 8 flexural dof's. All four types of discretization have boundary conditions $u^1(0,t) = u^2(0,t) = u^2(L,t) \equiv 0$. The discretization (3,3,4) can include, in addition, the boundary conditions $u^1{}_{,S}(L,t) = u^2{}_{,SS}(0,t) = u^2{}_{,SS}(L,t) \equiv 0$. It can be seen from Table 5.1 that the best results are obtained with a spatial discretization of type (3,3,4). So using (N^1, N^2) = (3,4), we not only achieve continuity of the necessary derivatives, but obtain more accurate frequencies than using (N^1, N^2) = (1,2). □ •

Example 5.2. Growth of energy and proposed treatment. Here is an example where without the special treatment in Step 5 and Step 6 of Algorithms **1** and **2**, one could encounter an undesirable growth in the offset of energy balance. Consider the

Maglev model B (Remark 3.1) with mass $M = 12{,}000kg$, and $I_w = \bar{R} = 0$. A vertical force of $F^2 = -600{,}000N$ is applied at its center of mass. The beam has the same properties as in Example 5.1. Let the system be driven by the initial conditions: $Y^1(0) = 0$, $\dot{Y}^1(0) = 30m/s$ ($\alpha = 0.256$), $\mathbf{u}(S,0) = \mathbf{u}_{,t}(S,0) \equiv 0$. 200 time steps with $h = 0.004s$ are used in the calculation.

Oscillations in numerical results. The time history of the nominal velocity $\dot{Y}^1(t)$ is plotted in Figure 5.2a: The solid line is the result obtained with Algorithm **2**; the dotted line is the result obtained if we do not reset the axial velocity and acceleration (Steps 5 and 6), and use (4.13a) to compute both the axial velocity and the transverse velocity. Oscillations in the dotted line appear very early, with increasing amplitude compared to the smoothness of the solid line. This oscillatory pattern is even more pronounced in the time histories of nominal acceleration (Figure 5.2b) and of energy balance (Figure 5.2c). We note that oscillations also occur in Algorithm **1**, with somewhat smaller amplitude, if the special treatment in Steps 5 and 6 is absent. Thus, the proposed algorithms effectively remove oscillations, which are clearly unacceptable. The offset in energy balance for Algorithm **2** (solid line in Figure 5.2c) is less than 0.0013% of the initial kinetic energy $\mathcal{K}_o$ ($= 5.4\times 10^6 kgm^2/s^2$). This offset is 0.0026% for Algorithm **1**, in agreement with our remark in the previous example.

Source of oscillations. The mechanism triggering the aforementioned oscillatory phenomenon can be explained by looking at the equations of motion (3.18) and (3.20a), recalling that $I_w = \bar{R} \equiv 0$. In particular, consider the axial acceleration $u^1{}_{,tt}$. This acceleration can be viewed as a driving force for the nominal motion, and is related to $\ddot{Y}^1$ by equation (3.18a). On the other hand, we consider the first term in equation (3.20a) — which contains $\ddot{Y}^1$ and $u^1{}_{,tt}(Y^1,t)$ — as a forcing term in solving for the predicted structural axial motion u^1. The numerical error thus acquired — mainly in the predictor stage — is then fed back to the nominal motion through the axial acceleration $u^1{}_{,tt}$ in equation (3.18a), as noted. Depending on the initial velocity $\dot{Y}^1(0)$, this error could

accumulate quickly, and grows in amplitude to create the observed oscillations. Moreover, oscillations arise more noticeably for larger ratio $M/A_\rho L$.

Finally, we note that parameters in the model could play a rôle in "dampening out" these oscillations: For instance, the case where the term I_w/R^2 in (3.18e) is non-zero (positive). Then the error fed back has diminishing influence on the vehicle motion — more so with larger value of I_w/R^2. It should be noticed that this type of energy growth does not occur to the transverse displacement u^2 for a similar reason: the presence of the factor $u^2{}_{,S} << 1$ of $u^2{}_{,tt}$ (see (3.18b)) as a "dampening" factor. In general, however, the proposed treatment of the axial acceleration during the predictor stage is an efficient way to eliminate oscillations. •

Example 5.3. High-speed vehicle on a six-span guideway: Energy transfer. The purpose of this example is to show the effect of vehicle/structure interaction on a long guideway. We consider here a similar situation as in Example 5.1, except that the structure is a six-span continuous beam, each span of $L = 24m$. Other parameters of the model are identical to those in Example 5.1, except that here $\overline{R} = 0$. The maximum static deflection is reduced from $L/140$ to about $L/200$. The boundary conditions here are such that $u^1(0,t) = u^2(kL,t) = 0$ for $k = 0,1,...,6$, and $u^1{}_{,S}(6L,t) = u^2{}_{,SS}(0,t) = u^2{}_{,SS}(6L,t) = 0$. Each span of the beam is modeled by one element of the type $(N^1, N^2) = (3,3)$, which allows discontinuity of $u^2{}_{,SSS}$ (related to shear force) at the supports. The initial velocity is set to $\dot{Y}^1(0) = 100m/s$. From experience in Example 5.1, 600 time steps (or 100 steps per span) are used to cover the traversing time on rigid guideway of $1.44s$, i.e., $h = 0.0024s$.

Nominal velocity. The vehicle nominal velocity drops steadily to a significant amount (Figure 5.3a). At the exit, this drop is about 3.5% of the initial velocity. Also, the computed nominal velocity with this discretization differs little from that obtained with a finer space-time discretization (two elements per span, and $h = 0.0012s$), as seen from Figure 5.3a.

Energy balance. The observed drop in nominal velocity is a result of energy transfer from the vehicle to the guideway, see Figure 5.3b. The loss in wheel kinetic energy is about 6.3% of the initial value. In Algorithm **2**, the offset in energy balance is less than 0.018% of the initial kinetic energy $\mathbb{K}_o$ ($= 22.5\times 10^6 kgm^2/s^2$); this offset is about 0.031% of $\mathbb{K}_o$ for Algorithm **1**. It is interesting to note that if the guideway (a multiple-span structure, but not necessarily continuous) is sufficiently long, a vehicle moving under its initial speed and its own weight, without other external force, will experience a continuous drop in speed due to energy transfer, even in the absence of any energy-dissipative mechanism such as mechanical friction or aerodynamic drag.

Influence lines. Dynamic influence lines at mid-span (beam mid-span deflection vs. vehicle nominal position) are given in Figure 5.3c for the first span, and in Figure 5.3d for the last span, together with the corresponding static influence lines. In the first span, there is a characteristic delay in the dynamic response at the beginning, and a sustained motion toward the end of the traversing, instead of a "motion" whose amplitude dies out quickly as in the static case (Figure 5.3c). In the sixth span, on the other hand, the response begins to build up quickly, with increasing amplitude, as soon as the vehicle enters the third span (Figure 5.3d). This amplitude build-up could be explained by the fact that the initial value of $\alpha = 0.854$ is close to the critical value of 1.† However, as noted above, for a sufficiently long continuous guideway and without the aid of any other external force, this amplitude growth in structural motion could not become unbounded because of the continuing loss in vehicle kinetic energy.

Contact force. We have in this example a case where the contact force $|F_c^2|$ reaches 2.5 times the vertical force $|F^2|$ (Figure 5.3e). Again, this points to the importance of the inertia term $M\ddot{u}^2$, which must be retained if the equation for nominal motion is to be valid at high speed, as noted in Remark 3.2. The horizontal contact

† For this type of resonance, we refer to Smith, Gilchrist & Wormley [1975] where the case of a moving force with constant speed is studied.

force F_c^1, has a maximum value of about 10% of the vertical force $|F^2|$ (Figure 5.3f).

Remark 5.2. The eigen-frequencies of the six-span beam used in this example are reported in the Table 5.2.

Table 5.2. *Eigen-frequencies of six-span beam.*

Frequency	Computed Values (Hz)	λ_i in (5.4)	
		Computed	Exact
f_1^1	3.4722	—	—
f_2^1	10.4167	—	—
f_1^2	2.4409	3.143	3.142
f_2^2	2.6295	3.262	3.261
f_3^2	3.1293	3.558	3.556
f_4^2	3.8165	3.930	3.927
f_5^2	4.5747	4.302	4.298
f_6^2	5.2485	4.608	4.601
f_7^2	9.8360	6.309	6.283
f_8^2	10.2467	6.439	6.410
f_9^2	11.2498	6.747	6.708
f_{10}^2	12.5411	7.124	7.069

The exact values of the axial frequencies f_i^1 and of the flexural frequencies f_i^2 are given according to

$$f_i^1 = \frac{(2i-1)}{4(6L)}\left(\frac{EA}{A_\rho}\right)^{\frac{1}{2}}, \quad f_i^2 = \frac{(\lambda_i)^2\pi}{2L^2}\left(\frac{EI}{A_\rho}\right)^{\frac{1}{2}}, \tag{5.4}$$

where the values of λ_i can be found in Smith, Gilchrist & Wormley [1975]. □ •

Example 5.4. Effects of braking on vehicle/structure system. The same model parameters as those in Example 5.3 are used here, except $\overline{R} = 0.9m$. We consider the effects of applying the following braking torque

$$T(t) = \begin{cases} -27{,}000t \ \ (Nm) & \text{for } t \in [0,\ 0.1] \\ -2{,}700 \ \ (Nm) & \text{for } t > 0.1s \end{cases} \tag{5.5}$$

to the wheel. On a rigid structure, the full torque creates a deceleration of $2m/s^2$. References on analysis of braking effects of vehicle on bridge can be found, e.g., in Gupta

& Traill-Nash [1980], and Lex-Mulcahy [1983]. Note that the vehicle models in these references have no mass in direct contact with the structure, and hence are simpler to handle. However, application of braking torque is not possible in these models.

Nominal velocity. Results are given for three initial velocities: $50m/s$, $75m/s$, and $100m/s$. From Figures 5.4a-c, one observes the increasingly pronounced effects of structure flexibility with increasing vehicle speed, as compared with the case of braking on a rigid structure. For the cases with $\dot{Y}^1(0) = 50m/s$ and $75m/s$, the nominal velocity follows more or less that obtained on a rigid structure (Figure 5.4a-b). By contrast, the case with $\dot{Y}^1(0) = 100m/s$ leads to a significant difference in the results (Figure 5.4c). Compared with the drop in velocity at exit of a rigid structure, the structure flexibility induces an additional drop of about 7% for $\dot{Y}^1(0) = 50m/s$ (Figure 5.4a), 16% for $\dot{Y}^1(0) = 75m/s$ (Figure 5.4b), and a sharply larger amount of 140% for $\dot{Y}^1(0) = 100m/s$ (Figure 5.4c: The exit velocity is $93.4m/s$ on flexible structure, compared with $97.2m/s$ on rigid structure). We note that, in traditional analysis of vehicle/structure interaction, the prescribed nominal velocity would coincide with that on a rigid structure.

Contact force. Had we prescribed the vehicle nominal motion to be the same as that on a rigid structure, this would result in a drastic difference in the magnitude of horizontal contact force: For initial velocities of $\dot{Y}^1(0) = 75m/s$ and $100m/s$, compare respectively Figures 5.4d and 5.4f (unknown nominal motion) with Figures 5.4e and 5.4g (prescribed nominal motion). Figures 5.4f and 5.4g are plotted at different scales to reveal a shifting pattern of the average contact force in Figure 5,4f, as a result of vehicle/structure interaction at high speed. For lower speed, this contact force does not depart significantly from the case of traversing a rigid structure (Figure 5.4d). The reason for the much larger horizontal contact force in the prescribed nominal motion case (3 to 4 times the contact force for unknown nominal motion) is due to the extra constraint forces that must be applied on the vehicle to make it follow the prescribed motion. •

6. Closure

We have presented a methodology for analyzing the interaction between high-speed vehicles and supporting flexible structures. The present approach departs completely from traditional practice of assuming known vehicle motion. Nonlinear equations of motion for a basic model, with a general form of contact constraint and valid for large structural deformation, are derived using Hamilton's principle. Additional assumptions, essentially on small structural deformation, are introduced to simplify these equations to a mildly nonlinear form. We propose efficient numerical algorithms to integrate the system of DAE's resulting from applying Galerkin spatial discretization.

Several examples are presented to illustrate the proposed approach. Discrete energy balance check, monitoring the numerical results, testifies to the reliability of these results, and therefore the viability of the method. We have shown some significant differences in the results, compared to those obtained in an analysis where vehicle nominal motion is prescribed. Further, energy transfer from the traversing vehicle to the supporting structure — decrease in vehicle kinetic energy, increase in energy stored in the structure, and balance of system energy — is clearly demonstrated. We thus effectively resolve the Timoshenko paradox in the spirit of Maunder [1960].

The present basic model is applicable to both wheel-on-rail and Maglev vehicles, and serves as a building block for general vehicle/structure models. The proposed numerical integration algorithms are not restricted to the basic model, but are as well applicable in this general situation.

Acknowledgements

We appreciate many enjoyable discussions with Dr. C. Hoff during the course of this research. The kind encouragement of Profs. R.L. Taylor, J.C. Simo, and Dr. J.E. Higgins, as well as the support from The Sweden-America Foundation to M. Olsson, are gratefully acknowledged.

References

Alscher, H., Iguchi, M., Eastham, A.R., and Boldea, I. [1983], "Non-contact suspension and propulsion technology," *Vehicle System Dynamics*, Vol. 12, pp. 259-289.

Belytschko, T. [1983], "Overview of semidiscretization," in *Computational Methods for Transient Analysis*, Vol. 1 of series in *Computational Methods in Mechanics*, edited by T. Belytschko and T.J.R. Hughes, North Holland Elsevier Science Publishers, Amsterdam.

Bettis, D.G. [1973], "A Runge-Kutta-Nyström algorithm," *Celestial Mechanics*, Vol. 8, pp. 229-233.

Blejwas, T.E., Feng, C.C., and Ayre, R.S. [1979], "Dynamic interaction of moving vehicles and structures," *J. Sound and Vibration*, Vol. 67, No. 4, pp. 513-521.

Butcher, J.C. [1987], *The Numerical Analysis of Ordinary Differential Equations*, John Wiley & Sons, New York.

Cherchas, D.B. [1979], "A dynamics simulation for a high speed magnetically levitated guided ground vehicle," *ASME J. Dynamic Systems, Measurements, and Control*, Vol. 101, No. 3, pp. 223-229.

Dekker, K., and Verwer, J.G. [1984], *Stability of Runge-Kutta Methods for Stiff Nonlinear Differential Equations*, CWI Monograph 2, North-Holland, Elsevier Science.

Deuflhard, P. [1985], "Recent progress in extrapolation methods for ordinary differential equations," *SIAM Review*, Vol. 27, No. 4, pp. 505-535.

Dormand, J.R., and Prince, P.J. [1978], "New Runge-Kutta algorithms for numerical simulation in dynamical astronomy," *Celestial Mechanics*, Vol. 18, pp. 223-232.

Eastham, A.R., and Hayes, W.F. [1987], "The status of development of Maglev systems," in Proc. of the *37th IEEE Vehicular Technology Conference*, Tampa, Florida, June, pp. 231-239.

Frýba, L. [1972], *Vibration of Solids and Structures under Moving Loads*, Noordhoff International Publishing, Groningen.

Führer, C. [1986], "Numerical integration methods in vehicle dynamics simulation," Proc. of the *3rd ICTS Course and Seminar on Advanced Vehicle System Dynamics*, Amalfi, Italy, May, pp. 329-345.

Führer, C., and Wallrapp, O. [1984], "A computer-oriented method for reducing linearized multibody system equations by incorporating constraints, *Comp. Meth. Appl. Mech. Engng.*, Vol. 46, pp. 169-175.

Gear, C.W. [1971], *Numerical Initial Value Problems in Ordinary Differential Equations*, Prentice-Hall, New York.

Gear, C.W. [1980], "Runge-Kutta starters for multistep methods," *ACM Transaction on Mathematical Software*, Vol. 6, pp. 263-279.

Gellert, M. [1978], "A new algorithm for integration of dynamic systems," *Computers &*

Structures, Vol. 9, pp. 401-408.

Gupta, G.K. [1980], "A note about overhead costs in ODE solvers," *ACM Transaction on Mathematical Software*, Vol. 6, No. 3, pp. 319-326.

Gupta, G.K., Sacks-Davis, R., and Tischer, P.E. [1985], "A review of recent developments in solving ODEs," *ACM Computing Surveys*, Vol. 17, No. 1, pp. 5-47.

Gupta, R.K., and Traill-Nash, R.W. [1980], "Bridge dynamic loading due to road surface irregularities and braking of vehicle," *Earthq. Engng. and Struct. Dyn.*, Vol. 8, pp. 83-96.

Hilber, H.M., Hughes, T.J.R., and Taylor, R.L. [1977], "Improved numerical dissipation for time integration algorithms in structural dynamics," *Earthq. Engng. & Struct. Dyn.*, Vol. 5, pp. 283-292.

Hoff, C. [1986], *Dissipative Step-by-Step Integration Methods for Nonlinear Structures under Earthquake Loading* (in German), Doctoral Dissertation D83, Technical University of Berlin, West Germany.

Hoff, C., and Pahl, P.J. [1987], "Development of an implicit method with numerical dissipation from a generalized single step algorithm for structural dynamics," preprint, to appear in *Comp. Meth. Appl. Mech. Engng.*

Huang, T. [1976], "Vibration of bridges," *Shock and Vibration Digest*, Vol. 8, No. 3, pp. 61-76.

Hughes, T.J.R. [1983], "Analysis of transient algorithms with particular reference to stability behavior," in *Computational Methods for Transient Analysis*, Vol. 1 of series in *Computational Methods in Mechanics*, edited by T. Belytschko and T.J.R. Hughes, North Holland Elsevier Science Publishers, Amsterdam.

Kalker, J.J. [1979], "Survey of wheel-rail rolling contact theory," *Vehicle System Dynamics*, Vol. 5, pp. 317-358.

Katona, M.G., and Zienkiewicz, O.C. [1985], "A unified set of single step algorithms. Part 3: The beta-*m* method, a generalization of the Newmark scheme," *Int. J. Num. Meth. Engng.*, Vol. 21, pp. 1345-1359.

Kortüm, W., and Wormley, D.N. [1981], "Dynamic interaction between travelling vehicles and guideway systems," *Vehicle System Dynamics*, Vol. 10, pp. 285-317.

Kortüm, W. [1986], "Introduction to system-dynamics of ground vehicles," in Proc. of the *3rd ICTS Course and Seminar on Advanced Vehicle System Dynamics*, Amalfi, Italy, May, pp. 1-36.

Lambert, J.D. [1973], *Computational Methods in Ordinary Differential Equations*, John Wiley & Sons, London.

Lawton, A. [1985], "Implementation of a Maglev vehicle suspension for flexible guideways," in Proc. of the *9th IASVD Symposium*, Linköping University, Linköping, Sweden, pp. 293-306.

Lex-Mulcahy, N. [1983], "Bridge response with tractor-trailer vehicle loading," *Earthq.*

Engng. and Struct. Dyn., Vol. 11, pp. 649-665.

Magrab, E.B. [1979], *Vibrations of Elastic Structural Members*, Sijthoff & Noordhoff, Alphen aan den Rijn.

Maunder, L. [1960], "On the work of a force crossing a beam," *Quart. of Applied Mathematics*, Vol. 17, pp. 437-440.

Nikravesh, P.E. [1984], "Some methods for dynamics analysis of constrained mechanical systems: A survey," in *Computer Aided Analysis and Optimization of Mechanical Systems*, edited by J. Haug, Springer, Berlin, pp. 351-368.

Olsson, M. [1985], "Finite element, modal co-ordinate analysis of structures subjected to moving loads," *J. Sound and Vibration*, Vol. 99, No. 1, pp. 1-12.

Olsson, M. [1986], *Analysis of Structures Subjected to Moving Loads*, Doctoral Dissertation, Report TVSM-1003, Division of Structural Mechanics, Lund University, Sweden.

Petzold, L.R. [1982], "A description of DASSL: A differential/algebraic system solver," in Proc. of the 10th IMACS *World Congress on System Simulation and Scientific Computation*, Montreal, August.

Raschbichler, H.G., and Wackers, M. [1987], "Status of the Maglev and linear drive technology program in the Federal Republic of Germany," *IEEE Int. Conf. on Maglev and Linear Drives*, Las Vegas, May, pp. 147-154.

Rektorys, K. [1980], *Variational Methods in Mathematics, Science, and Engineering*, D. Reidel Pub. Co., Dortrecht, Holland.

Simo, J.C., and Vu-Quoc, L. [1986], "On the dynamics of flexible beams under large overall motions — The plane case: Parts I and II," *ASME J. Applied Mechanics*, Vol. 53, No. 4, pp. 849-863.

Smith, C.C., Gilchrist, A.J., and Wormley, D.N. [1975], "Multiple and continuous span elevated guideway-vehicle dynamic performance," *ASME J. Dynamic Systems, Measurements, and Control*, Vol. 97, No. 1, pp. 30-40.

Stanisic, M.M. [1985], "On a new theory of the dynamic behaviour of the structures carrying moving masses," *Ingenieur-Archiv*, Vol. 55, pp. 176-185.

Subcommittee on Vibration Problems Associated with Flexural Members on Transit Systems, Structural Division [1985], "Dynamics of steel elevated guideways — An overview," *J. Structural Engineering*, Vol. 111, No. 9, pp. 1873-1898.

Ting, E.C., Genin, J., and Ginsberg, J.H. [1974], "A general algorithm for moving mass problems," *J. Sound and Vibration*, Vol. 33, No. 1, pp 49-58.

Ting, E.C., Genin, J., and Ginsberg, J.H. [1975], "Literature review — Dynamic interaction of bridge structures and vehicles," *Shock and Vibration Digest*, Vol. 7, No. 11, pp. 61-69.

Ting, E.C., and Yener, M. [1983], "Vehicle-structure interactions in bridge dynamics," *Shock and Vibration Digest*, Vol. 15, No. 12, pp. 3-9.

Trujillo, D.H. [1972], "An unconditionally stable explicit algorithm for structural dynamics," *Int. J. Num. Meth. Engng.*, Vol. 11, pp. 1579-1592.

Venancio-Filho, F. [1978], "Finite element analysis of structures under moving loads," *Shock and Vibration Digest*, Vol. 10, No. 8, pp. 27-35.

Vu-Quoc, L. [1986], *Dynamics of Flexible Structures Performing Large Overall Motions: A Geometrically-Nonlinear Approach*, Doctoral Dissertation, Electronics Research Laboratory Memorandum UCB/ERL M86/36, University of California, Berkeley.

Vu-Quoc, L., and Simo, J.C. [1987], "Dynamics of earth-orbiting satellites with flexible multibody components," to appear in *AIAA J. Guidance, Control, and Dynamics.*

Wallrapp, O. [1986], "Elastic vehicle guideway structures," in Proc. of the *3rd ICTS Course and Seminar on Advanced Vehicle System Dynamics*, Amalfi, Italy, May, pp. 215-232.

Wood, W.L. [1987], "Some transient and coupled problems — A state-of-the-art review," in *Numerical Methods for Transient and Coupled Problems*, edited by R.W. Lewis *et al*, John Wiley & Sons Ltd.

Zicha, J.H. [1986], "Civil aspects of Maglev design," *IEEE Int. Conf. on Maglev & Linear Drives*, Vancouver, Canada, May, pp. 69-87.

Zienkiewicz, O.C. [1977], *The Finite Element Method*, McGraw Hill, New York.

Figure captions

Figure 3.1. *Basic problem.* Model parameters.

Figure 5.0. *Basic vehicle/structure models.* Simple-span and six-span beam structures.

Figure 5.1a. *Vehicle/structure interaction at different initial velocities.* Nominal velocity vs. Time. Initial velocity $\dot{Y}^1(0) = 1m/s$. Beam length $L = 24m$.

Figure 5.1b. *Vehicle/structure interaction at different initial velocities.* Nominal velocity vs. Time. Initial velocity $\dot{Y}^1(0) = 10m/s$. Beam length $L = 24m$.

Figure 5.1c. *Vehicle/structure interaction at different initial velocities.* Nominal velocity vs. Time. Initial velocity $\dot{Y}^1(0) = 50m/s$. Beam length $L = 24m$.

Figure 5.1d. *Vehicle/structure interaction at different initial velocities.* Nominal velocity vs. Time. Initial velocity $\dot{Y}^1(0) = 100m/s$. Beam length $L = 24m$. Solid line: 200 time steps. Dotted line: 100 time steps.

Figure 5.1e. *Vehicle/structure interaction at different initial velocities.* Vertical displacement at contact point (normalized wrt $0.1728m$) vs. Nominal position. $\dot{Y}^1(0) = 1m/s, 10m/s, 50m/s, 100m/s$. $L = 24m$.

Figure 5.1f. *Vehicle/structure interaction at different initial velocities.* Vertical mid-span displacement (normalized wrt $0.1728m$) vs. Time (normalized wrt traversing time on rigid beam). $\dot{Y}^1(0) = 1m/s, 10m/s, 50m/s, 100m/s$. $L = 24m$.

Figure 5.1g. *Vehicle/structure interaction at different initial velocities.* Vertical contact force F_c^2 (normalized wrt vertical force F^2) vs. Time. $\dot{Y}^1(0) = 50m/s, 100m/s$.

Figure 5.1h. *Vehicle/structure interaction at different initial velocities.* Energy ($\times 10^6$) vs. Time. Initial velocity $\dot{Y}^1(0) = 10m/s$.

Figure 5.1i. *Vehicle/structure interaction at different initial velocities.* Energy balance ($\times 10^6$) vs. Time. Offset of energy at transition from Algorithm **1** to Algorithm **2**. $\dot{Y}^1(0) = 10m/s$. $h = 0.012s$.

Figure 5.1j. *Vehicle/structure interaction at different initial velocities.* Energy ($\times 10^6$) vs. Time. Initial velocity $\dot{Y}^1(0) = 100m/s$.

Figure 5.2a. *Growth of energy and proposed treatment.* Nominal velocity vs. Time. Solid line: Algorithm **2**. Dotted line: without treatment for axial motion.

Figure 5.2b. *Growth of energy and proposed treatment.* Nominal acceleration vs. Time. Solid line: Algorithm **2**. Dotted line: without treatment for axial motion.

Figure 5.2c. *Growth of energy and proposed treatment.* Energy balance ($\times 10^6$) vs. Time. Solid line: Algorithm **2**. Dotted line: without treatment for axial motion.

Figure 5.3a. *High-speed vehicle on a six-span guideway.* Nominal velocity vs. Time.

Figure 5.3b. *High-speed vehicle on a six-span guideway.* Energy vs. Time. Solid line: energy balance ($\times 10^6$). Dotted line: wheel kinetic energy.

Figure 5.3c. *High-speed vehicle on a six-span guideway.* Influence line: Vertical mid-span deflection in first span vs. Nominal position. Solid line: dynamic. Dotted line: static.

Figure 5.3d. *High-speed vehicle on a six-span guideway.* Influence line: Vertical mid-span deflection in 6th span vs. Nominal position. Solid line: dynamic. Dotted line: static.

Figure 5.3e. *High-speed vehicle on a six-span guideway.* Vertical contact force F_c^2 (normalized wrt vertical force F^2) vs. Time.

Figure 5.3f. *High-speed vehicle on a six-span guideway.* Horizontal contact force F_c^1 (normalized wrt vertical force $|F^2|$) vs. Time.

Figure 5.4a. *Effects of braking on vehicle/structure system.* Nominal velocity vs. Time. Six-span beam. Initial velocity $\dot{Y}^1(0) = 50m/s$.

Figure 5.4b. *Effects of braking on vehicle/structure system.* Nominal velocity vs. Time. Six-span beam. Initial velocity $\dot{Y}^1(0) = 75m/s$.

Figure 5.4c. *Effects of braking on vehicle/structure system.* Nominal velocity vs. Time. Six-span beam. Initial velocity $\dot{Y}^1(0) = 100m/s$.

Figure 5.4d. *Effects of braking on vehicle/structure system.* (Nominal motion as unknown.) Horizontal contact force F_c^1 (normalized wrt vertical force $|F^2|$) vs. Time. Solid line: flexible structure. Dotted line: rigid structure. $\dot{Y}^1(0) = 75m/s$.

Figure 5.4e. *Effects of braking on vehicle/structure system.* (Nominal motion as on rigid beam.) Horizontal contact force F_c^1 (normalized wrt vertical force $|F^2|$) vs. Time. Solid line: flexible structure. Dotted line: rigid structure. $\dot{Y}^1(0) = 75m/s$.

Figure 5.4f. *Effects of braking on vehicle/structure system.* (Nominal motion as unknown.) Horizontal contact force F_c^1 (normalized wrt vertical force $|F^2|$) vs. Time. Solid line: flexible structure. Dotted line: rigid structure. $\dot{Y}^1(0) = 100m/s$.

Figure 5.4g. *Effects of braking on vehicle/structure system.* (Nominal motion as on rigid beam.) Horizontal contact force F_c^1 (normalized wrt vertical force $|F^2|$) vs. Time. Solid line: flexible structure. Dotted line: rigid structure. $\dot{Y}^1(0) = 100m/s$.

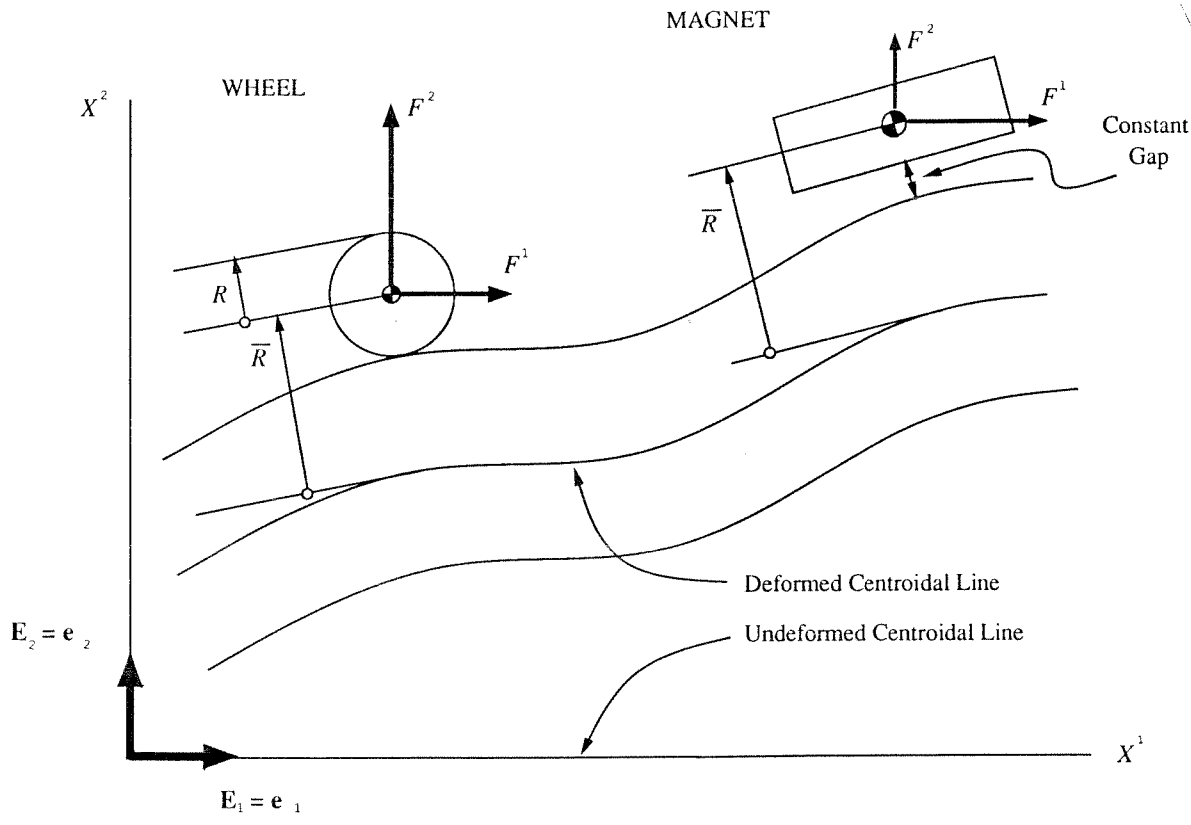

Figure 3.1. *Basic problem.* Model parameters.

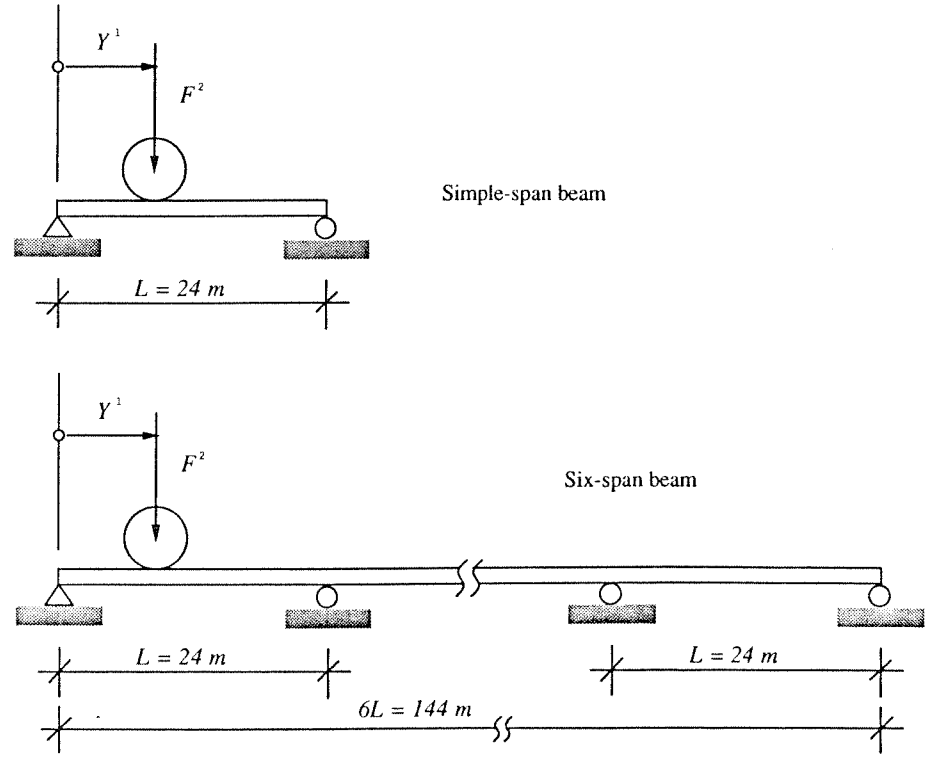

Figure 5.0. *Basic vehicle/structure models.* Simple-span and six-span beam structures.

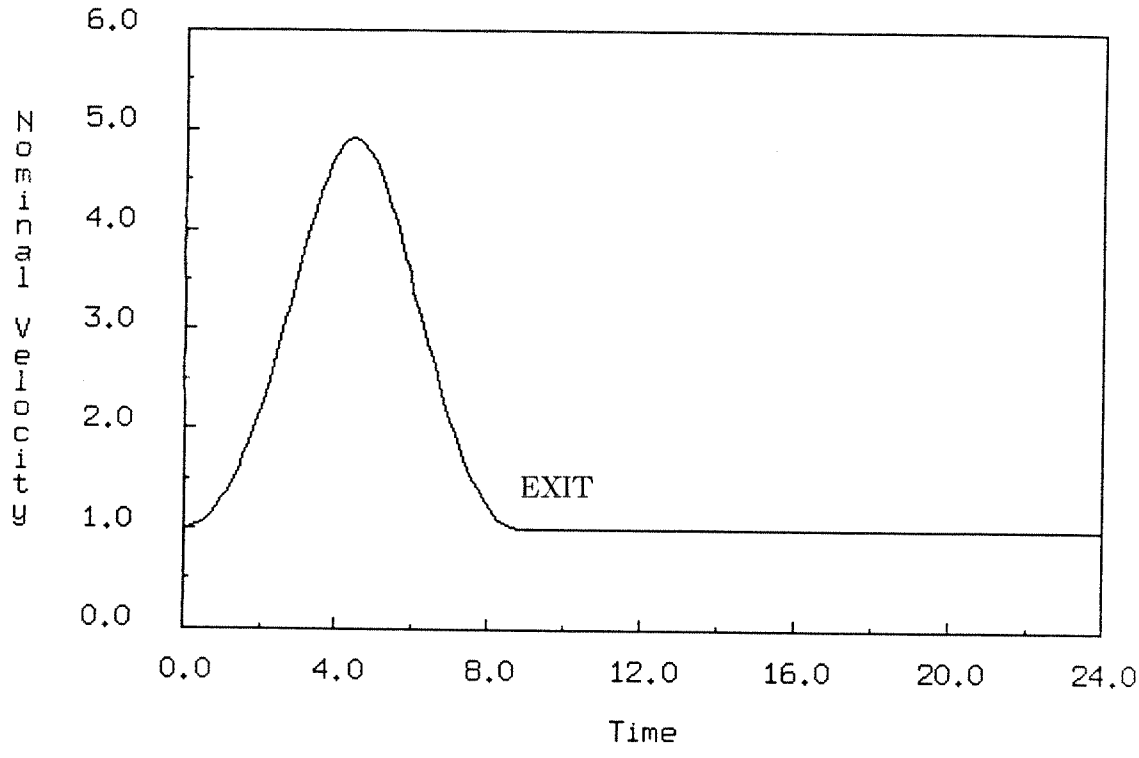

Figure 5.1a. *Vehicle/structure interaction at different initial velocities.* Nominal velocity vs. Time. Initial velocity $\dot{Y}^1(0) = 1m/s$. Beam length $L = 24m$.

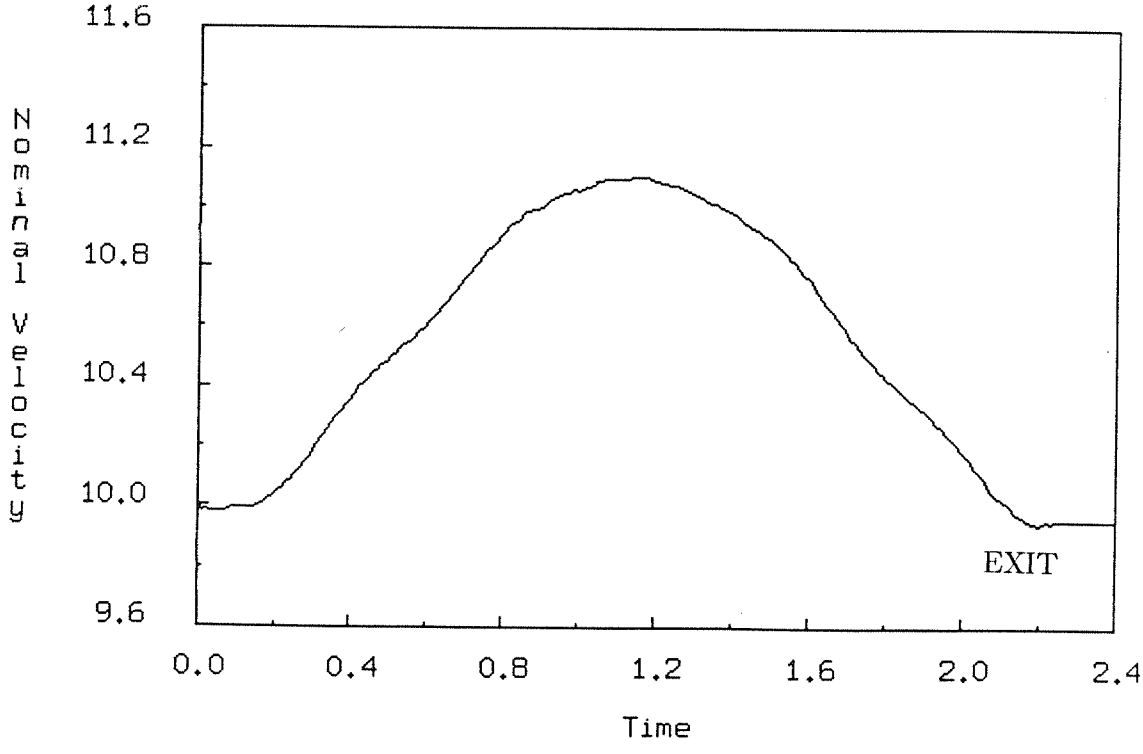

Figure 5.1b. *Vehicle/structure interaction at different initial velocities.* Nominal velocity vs. Time. Initial velocity $\dot{Y}^1(0) = 10m/s$. Beam length $L = 24m$.

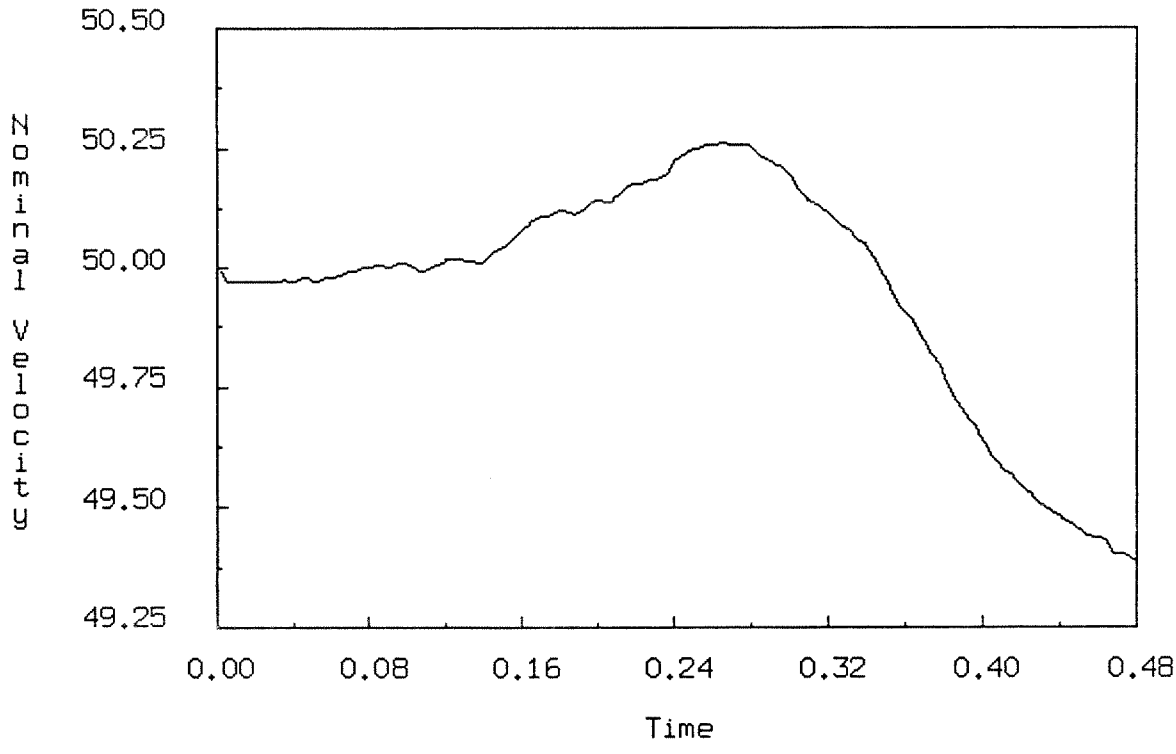

Figure 5.1c. *Vehicle/structure interaction at different initial velocities.* Nominal velocity vs. Time. Initial velocity $\dot{Y}^1(0) = 50m/s$. Beam length $L = 24m$.

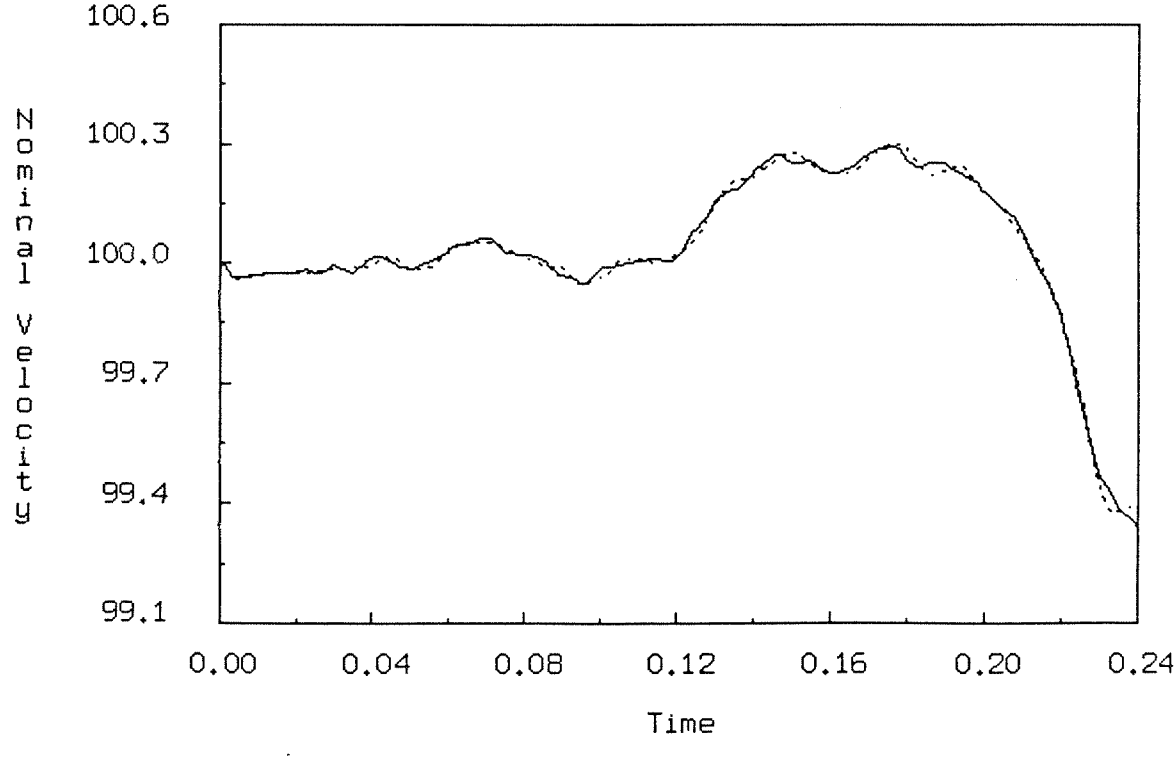

Figure 5.1d. *Vehicle/structure interaction at different initial velocities.* Nominal velocity vs. Time. Initial velocity $\dot{Y}^1(0) = 100m/s$. Beam length $L = 24m$. Solid line: 200 time steps. Dotted line: 100 time steps.

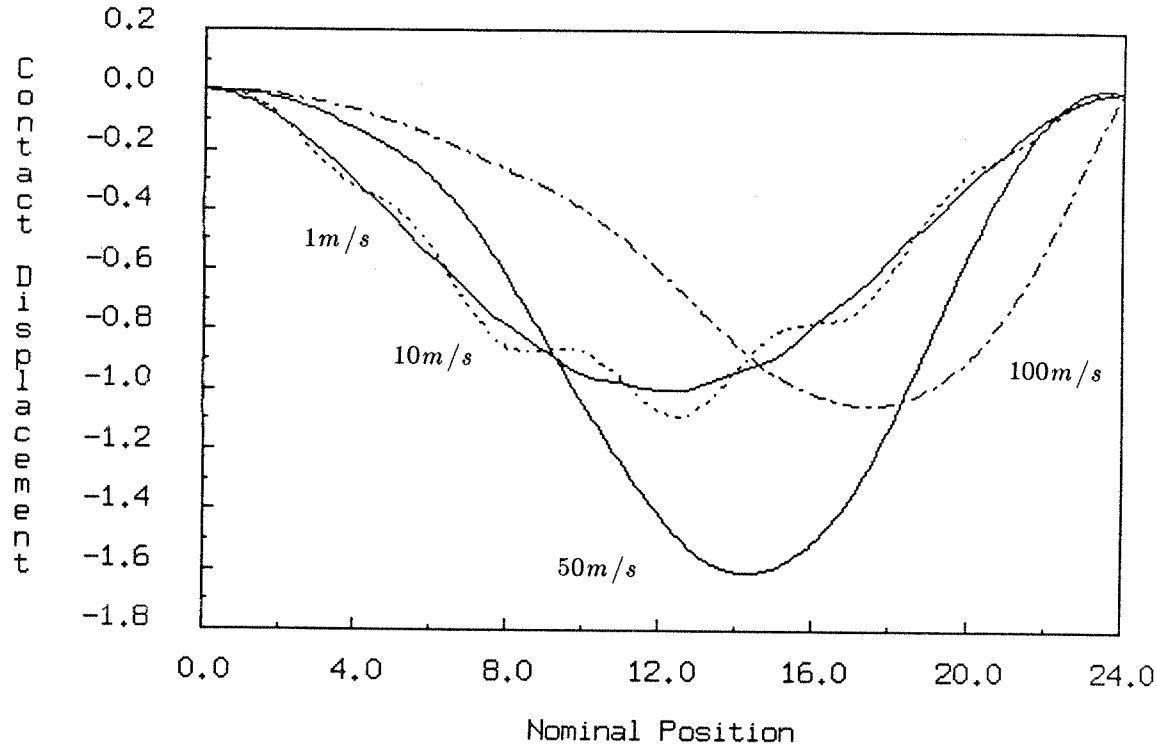

Figure 5.1e. *Vehicle/structure interaction at different initial velocities.* Vertical displacement at contact point (normalized wrt $0.1728m$) vs. Nominal position. $\dot{Y}^1(0) = 1m/s, 10m/s, 50m/s, 100m/s$. $L = 24m$.

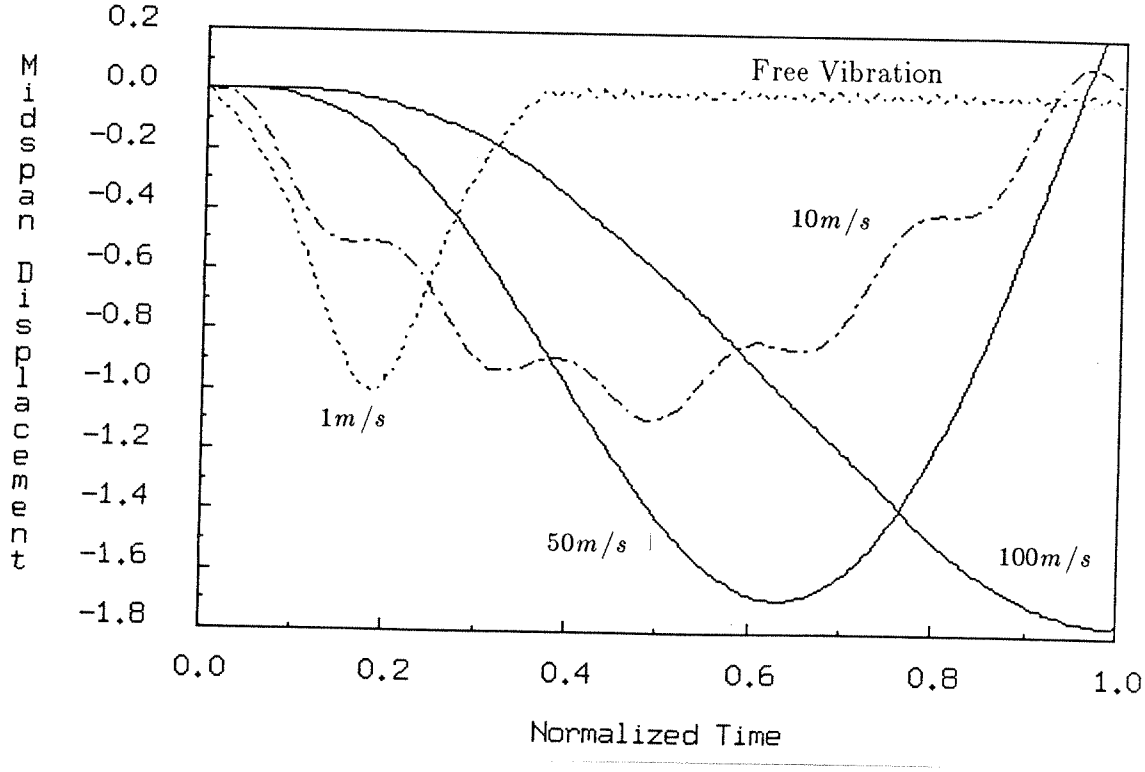

Figure 5.1f. *Vehicle/structure interaction at different initial velocities.* Vertical mid-span displacement (normalized wrt $0.1728m$) vs. Time (normalized wrt traversing time on rigid beam). $\dot{Y}^1(0) = 1m/s, 10m/s, 50m/s, 100m/s$. $L = 24m$.

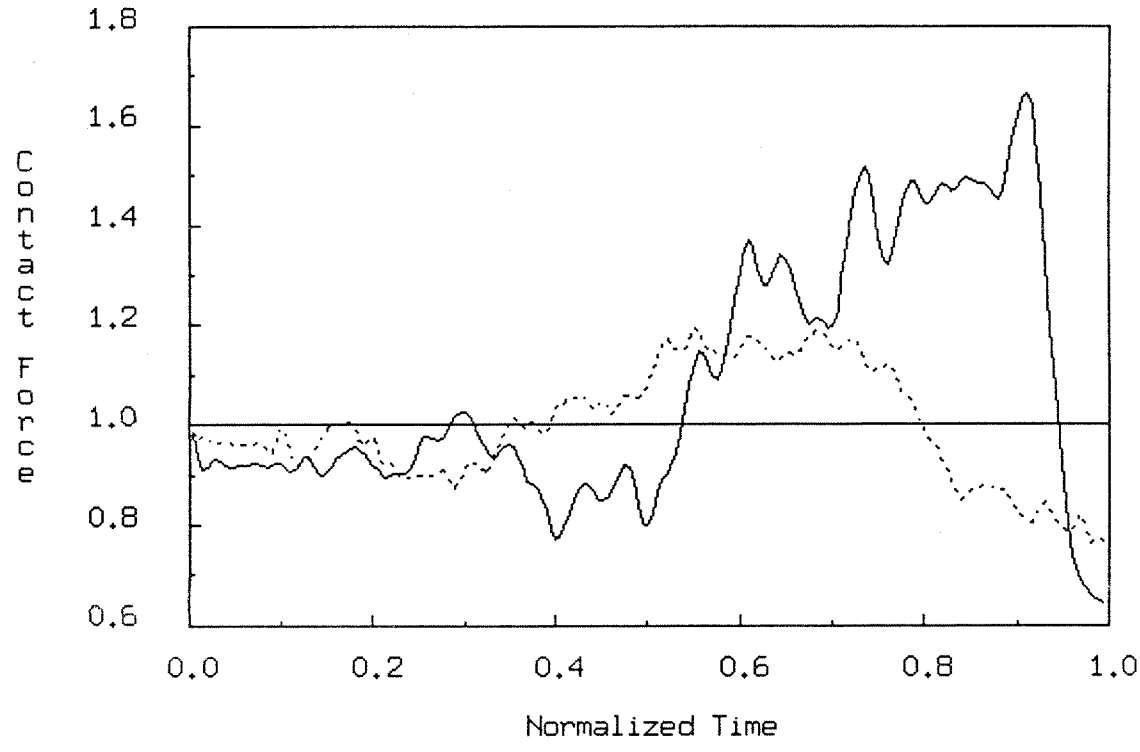

Figure 5.1g. *Vehicle/structure interaction at different initial velocities.* Vertical contact force F_c^2 (normalized wrt vertical force F^2) vs. Time. $\dot{Y}^1(0) = 50m/s, 100m/s$.

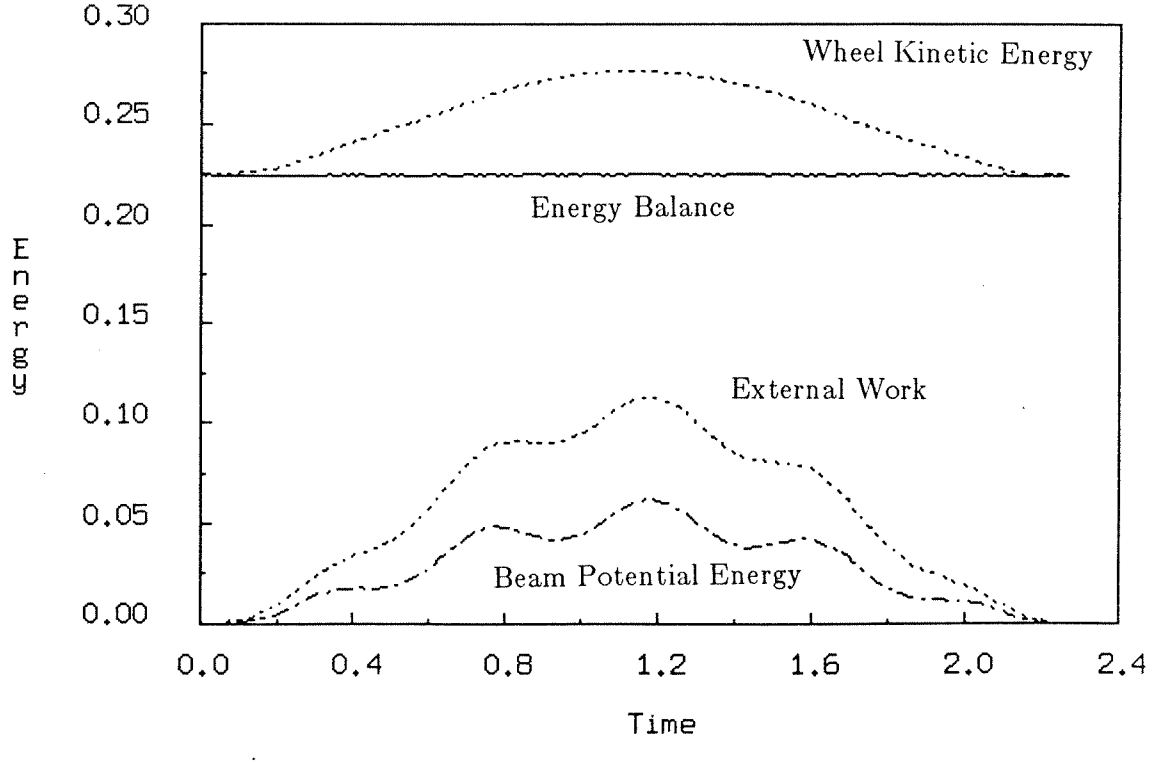

Figure 5.1h. *Vehicle/structure interaction at different initial velocities.* Energy ($\times 10^6$) vs. Time. Initial velocity $\dot{Y}^1(0) = 10m/s$.

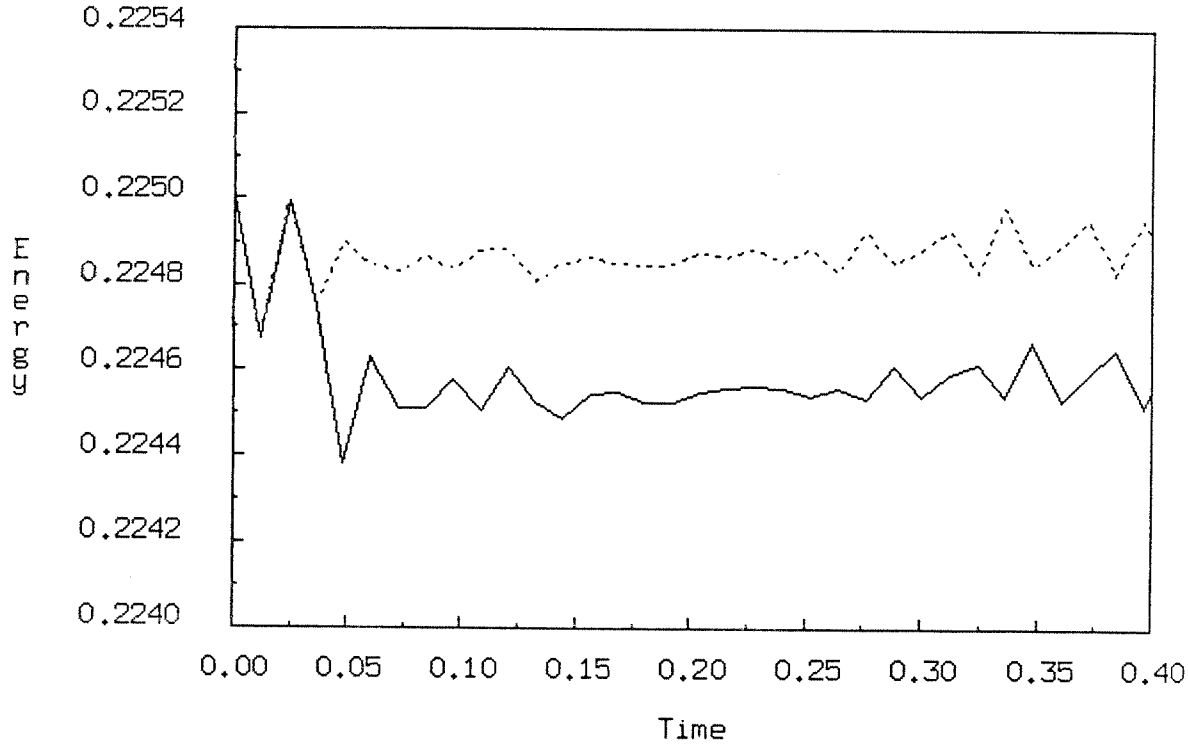

Figure 5.1i. *Vehicle/structure interaction at different initial velocities.* Energy balance ($\times 10^6$) vs. Time. Offset of energy at transition from Algorithm **1** to Algorithm **2**. $\dot{Y}^1(0) = 10m/s$. $h = 0.012s$.

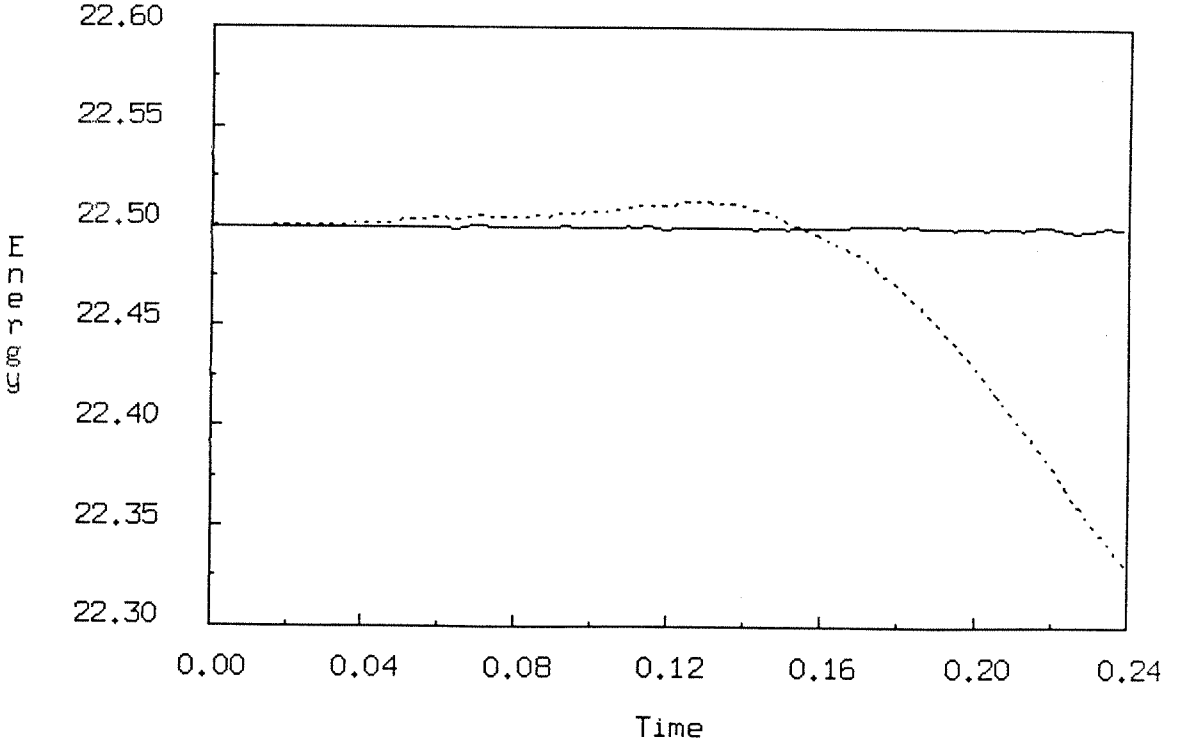

Figure 5.1j. *Vehicle/structure interaction at different initial velocities.* Energy ($\times 10^6$) vs. Time. Initial velocity $\dot{Y}^1(0) = 100m/s$.

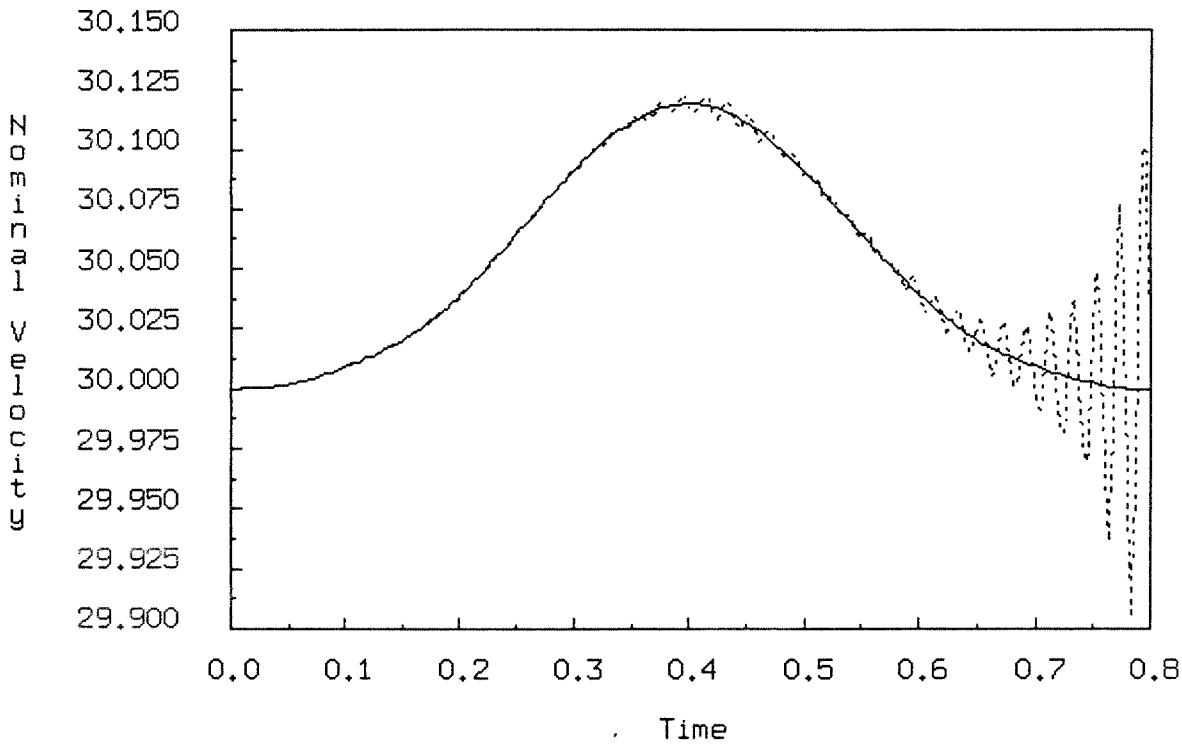

Figure 5.2a. *Growth of energy and proposed treatment.* Nominal velocity vs. Time. Solid line: Algorithm **2**. Dotted line: without treatment for axial motion.

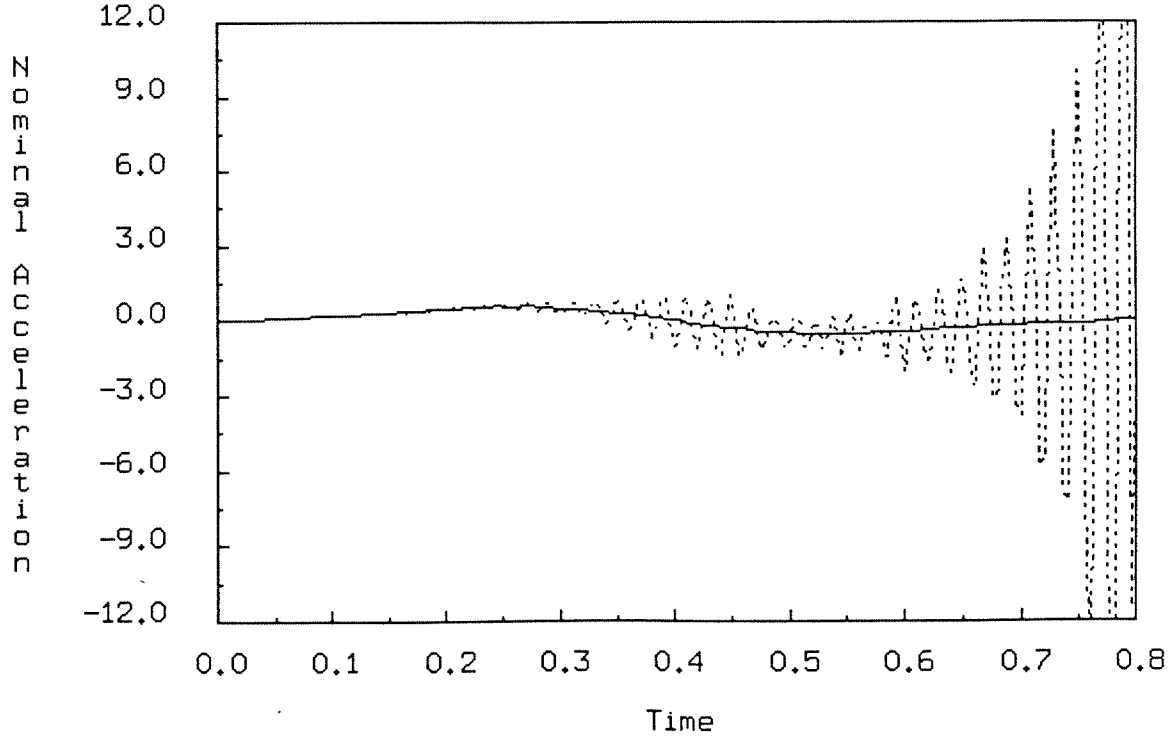

Figure 5.2b. *Growth of energy and proposed treatment.* Nominal acceleration vs. Time. Solid line: Algorithm **2**. Dotted line: without treatment for axial motion.

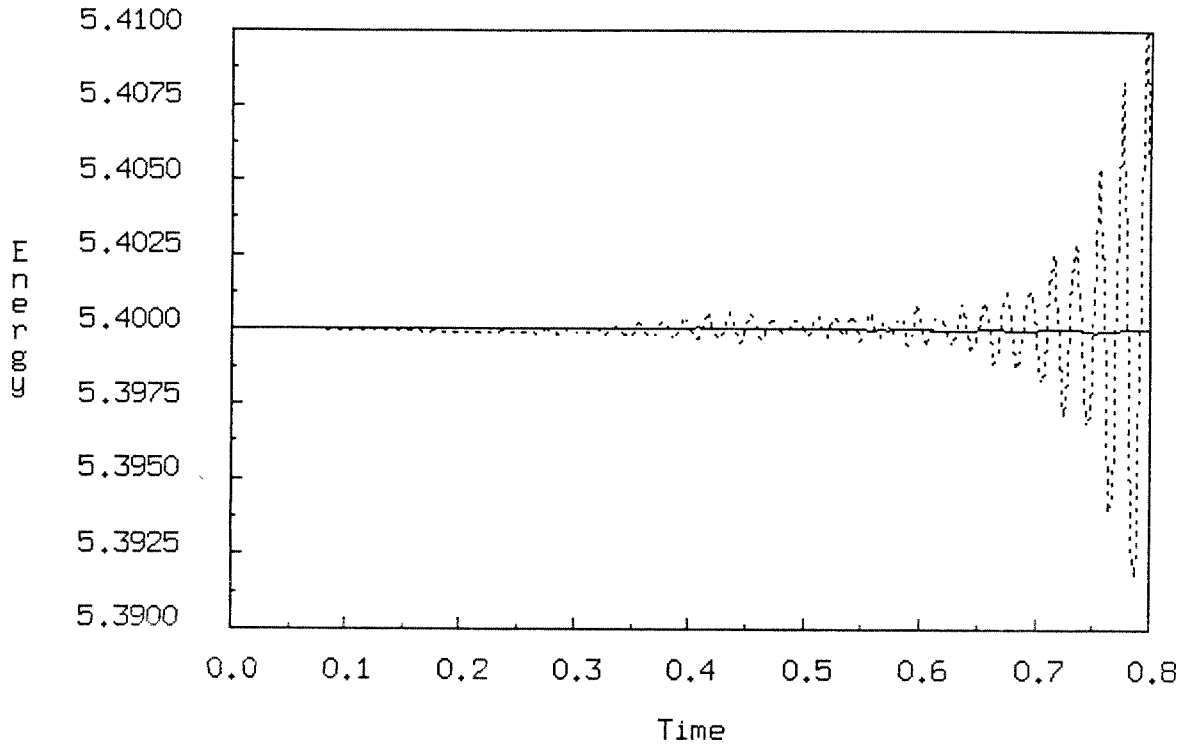

Figure 5.2c. *Growth of energy and proposed treatment.* Energy balance ($\times 10^6$) vs. Time. Solid line: Algorithm **2**. Dotted line: without treatment for axial motion.

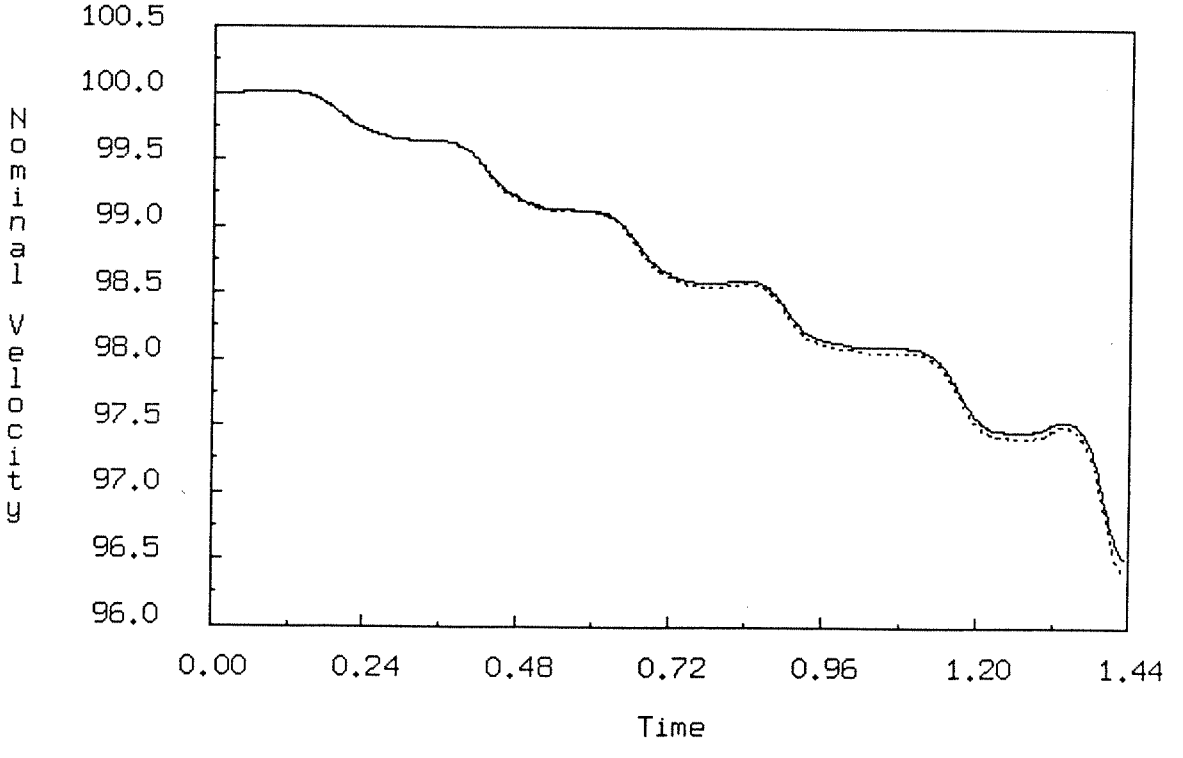

Figure 5.3a. *High-speed vehicle on a six-span guideway.* Nominal velocity vs. Time.

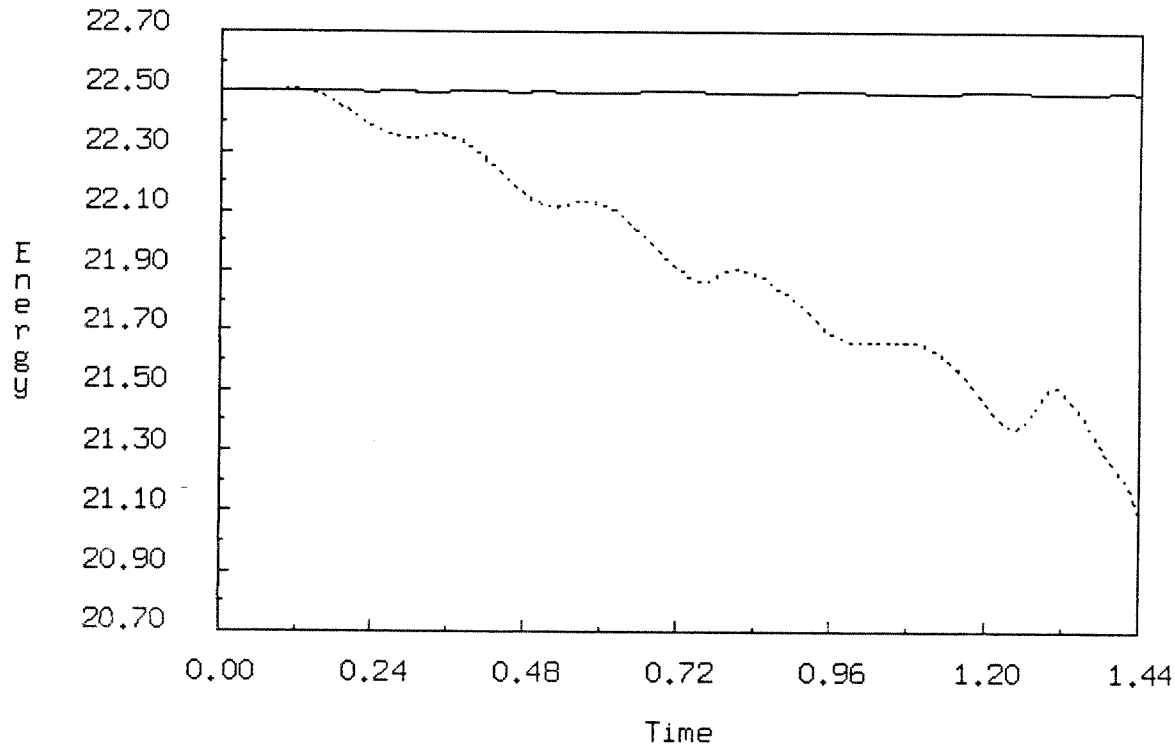

Figure 5.3b. *High-speed vehicle on a six-span guideway.* Energy vs. Time. Solid line: energy balance ($\times 10^6$). Dotted line: wheel kinetic energy.

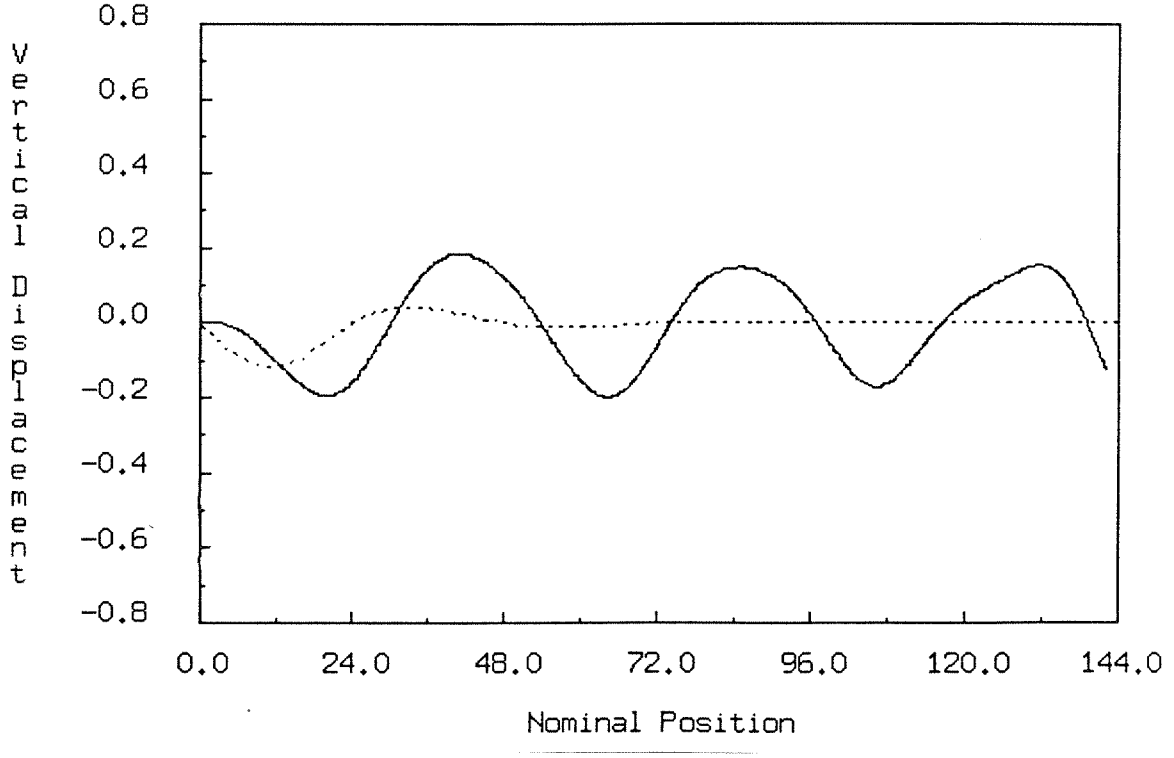

Figure 5.3c. *High-speed vehicle on a six-span guideway.* Influence line: Vertical mid-span deflection in first span vs. Nominal position. Solid line: dynamic. Dotted line: static.

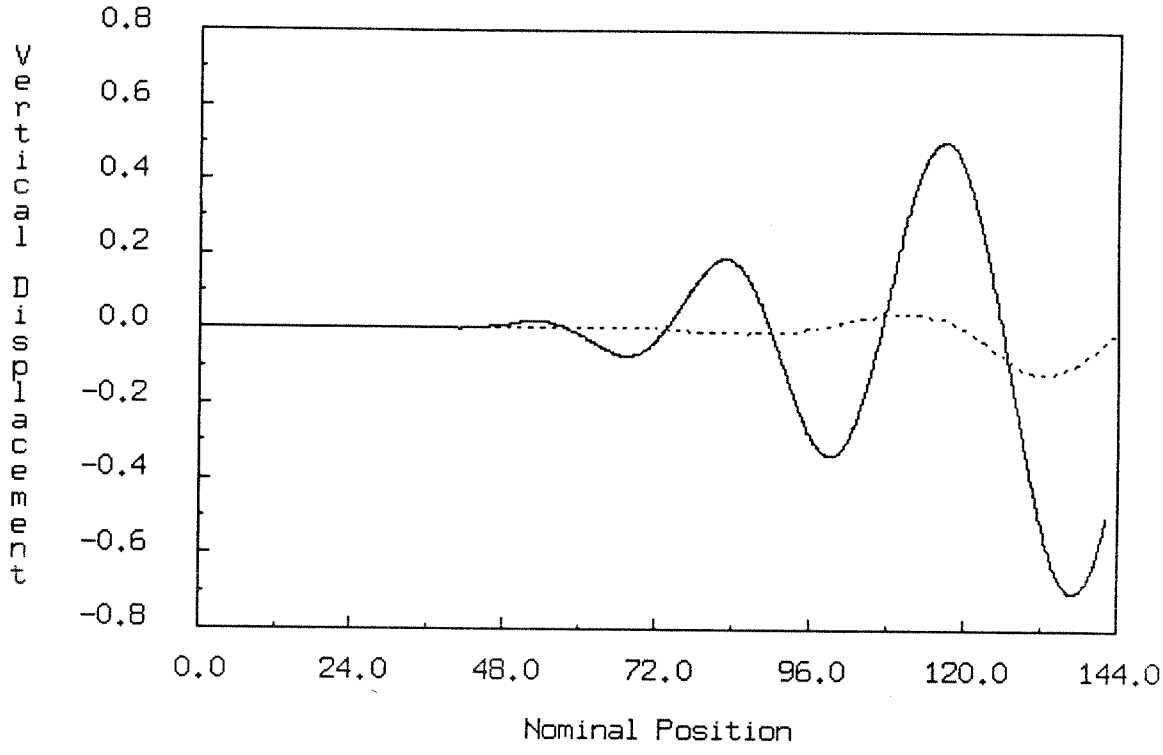

Figure 5.3d. *High-speed vehicle on a six-span guideway.* Influence line: Vertical mid-span deflection in 6th span vs. Nominal position. Solid line: dynamic. Dotted line: static.

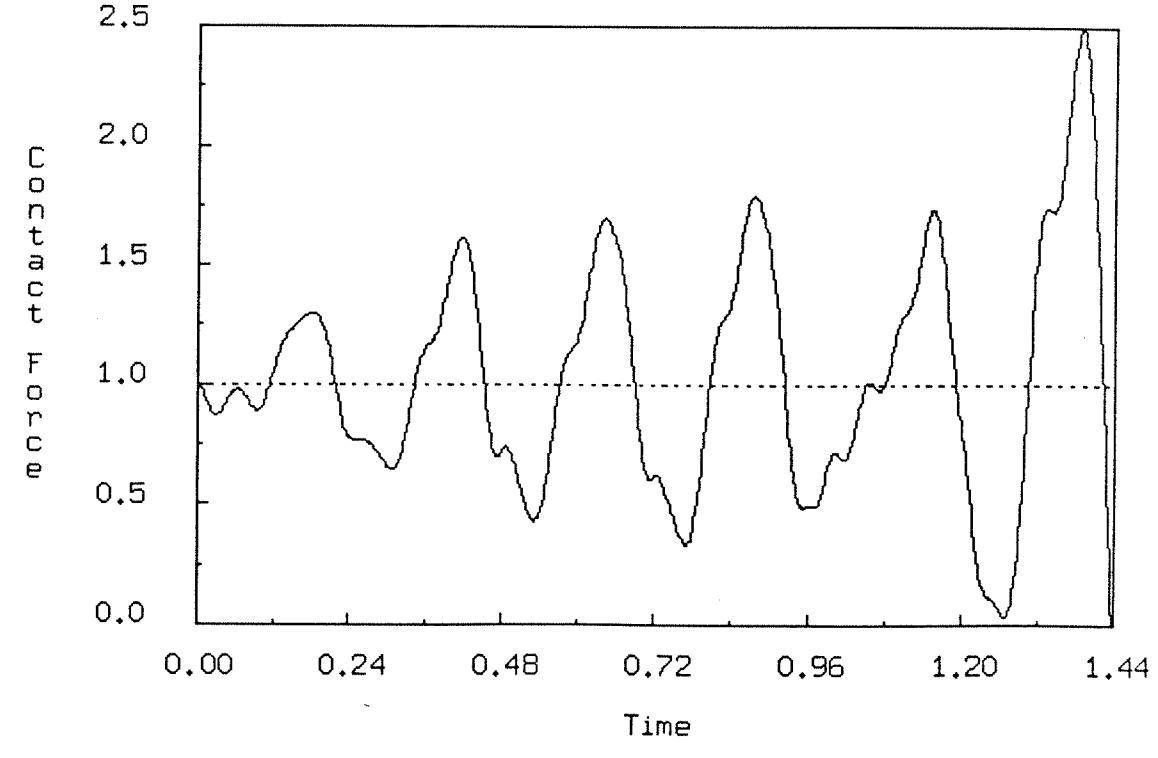

Figure 5.3e. *High-speed vehicle on a six-span guideway.* Vertical contact force F_c^2 (normalized wrt vertical force F^2) vs. Time.

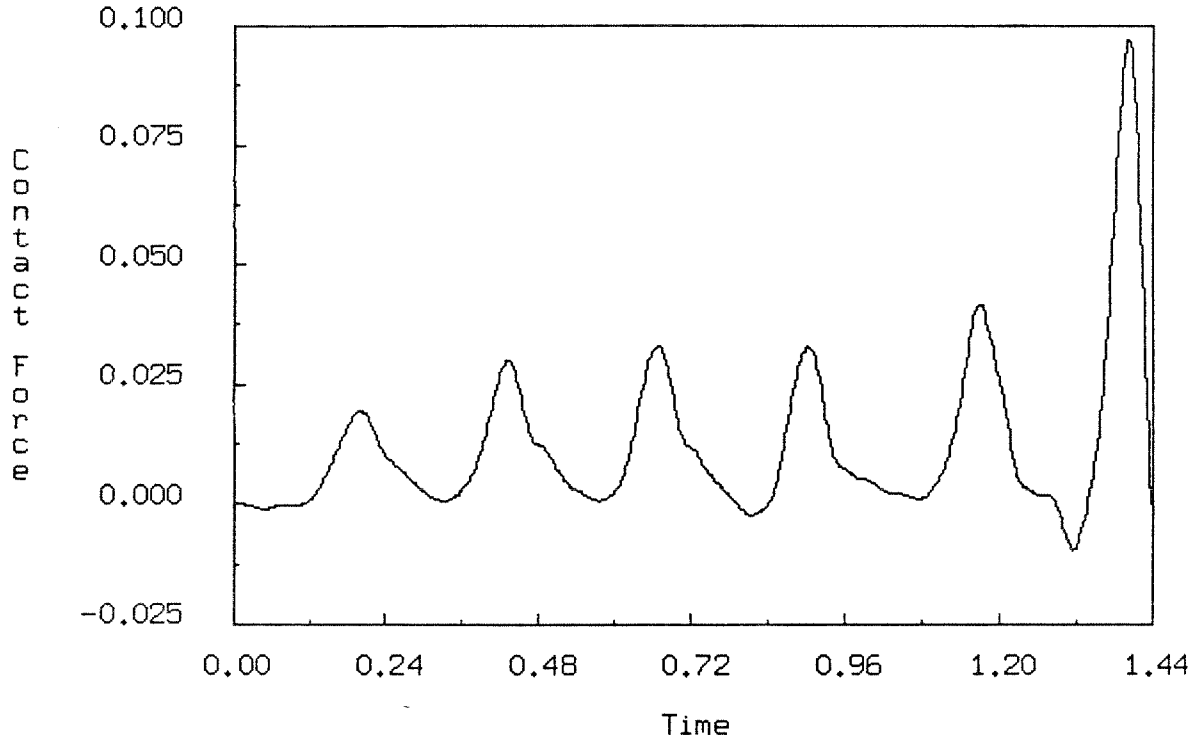

Figure 5.3f. *High-speed vehicle on a six-span guideway.* Horizontal contact force F_c^1 (normalized wrt vertical force $|F^2|$) vs. Time.

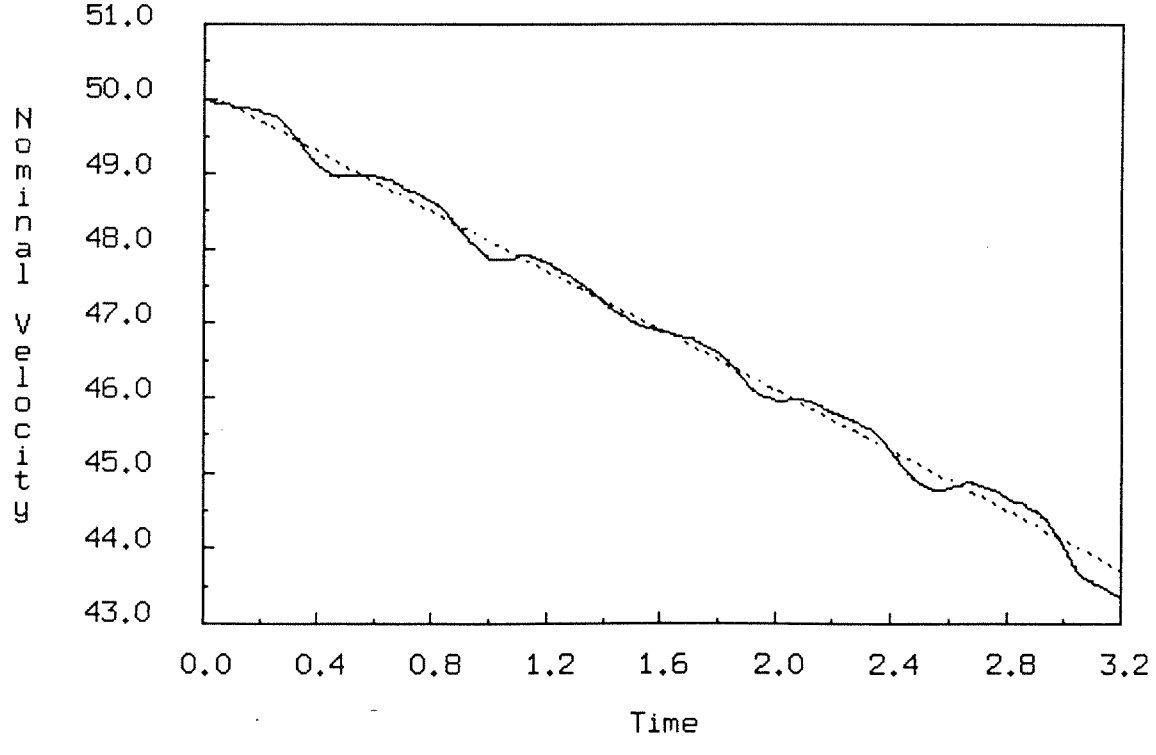

Figure 5.4a. *Effects of braking on vehicle/structure system.* Nominal velocity vs. Time. Six-span beam. Initial velocity $\dot{Y}^1(0) = 50m/s$.

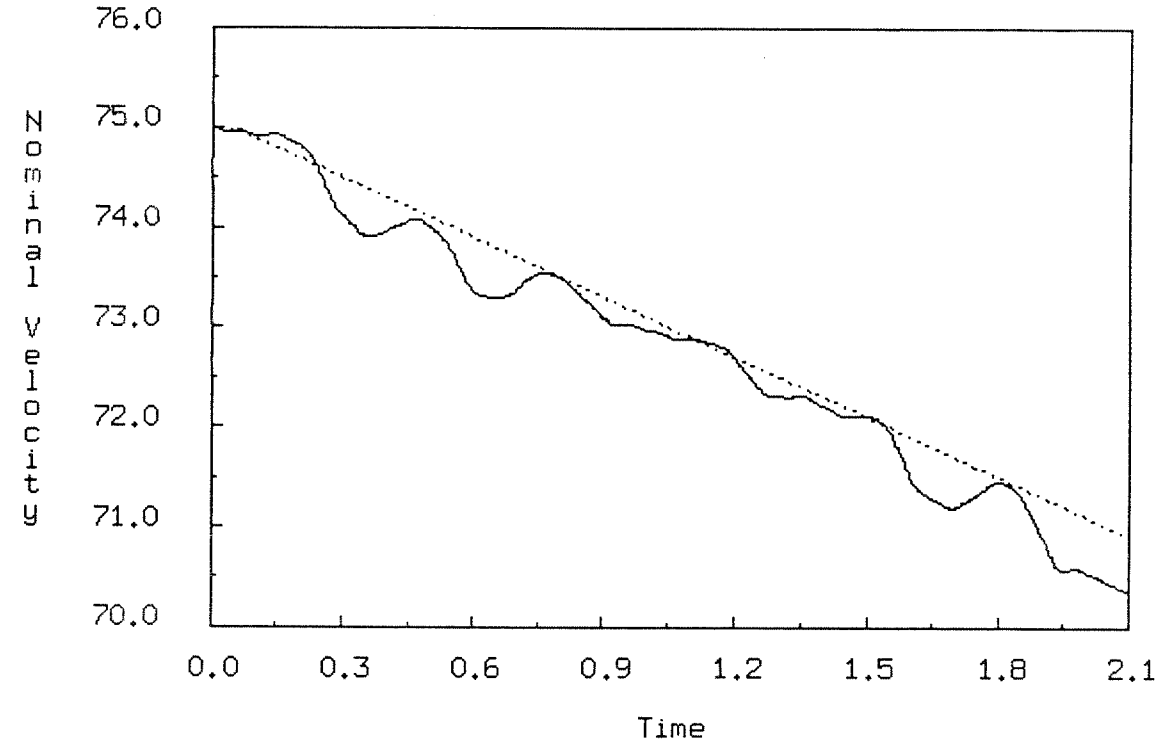

Figure 5.4b. *Effects of braking on vehicle/structure system.* Nominal velocity vs. Time. Six-span beam. Initial velocity $\dot{Y}^1(0) = 75m/s$.

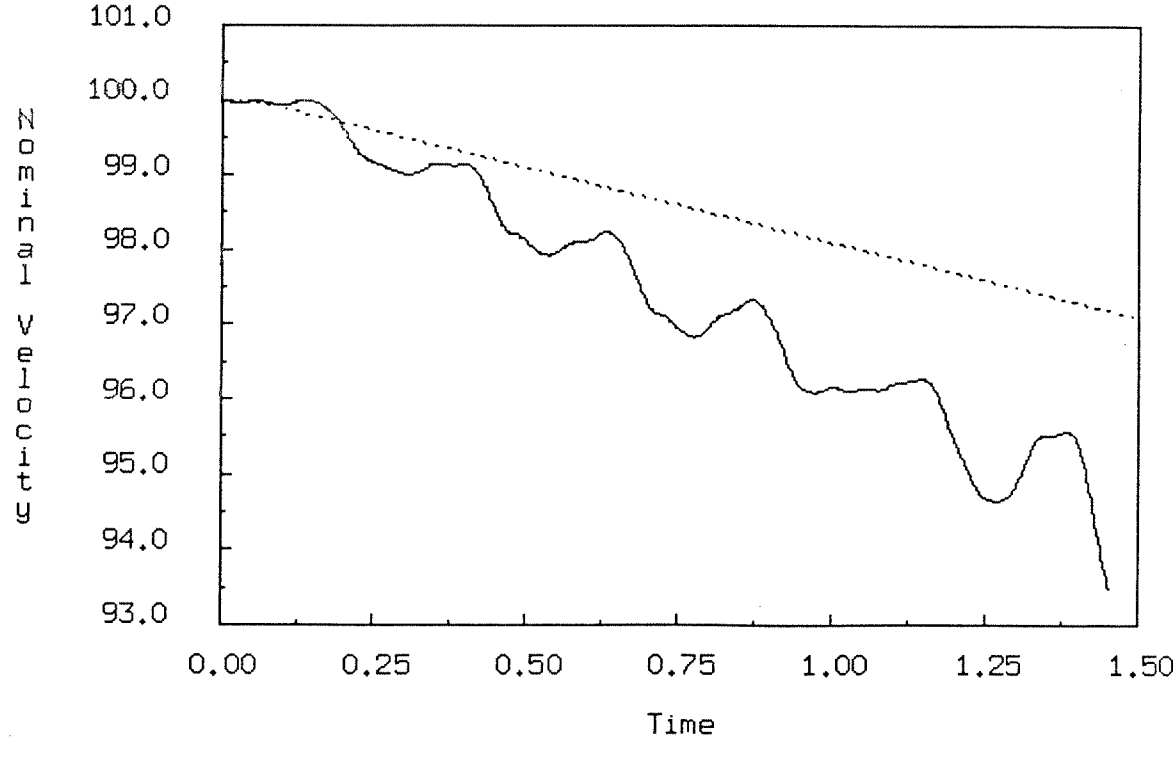

Figure 5.4c. *Effects of braking on vehicle/structure system.* Nominal velocity vs. Time. Six-span beam. Initial velocity $\dot{Y}^1(0) = 100m/s$.

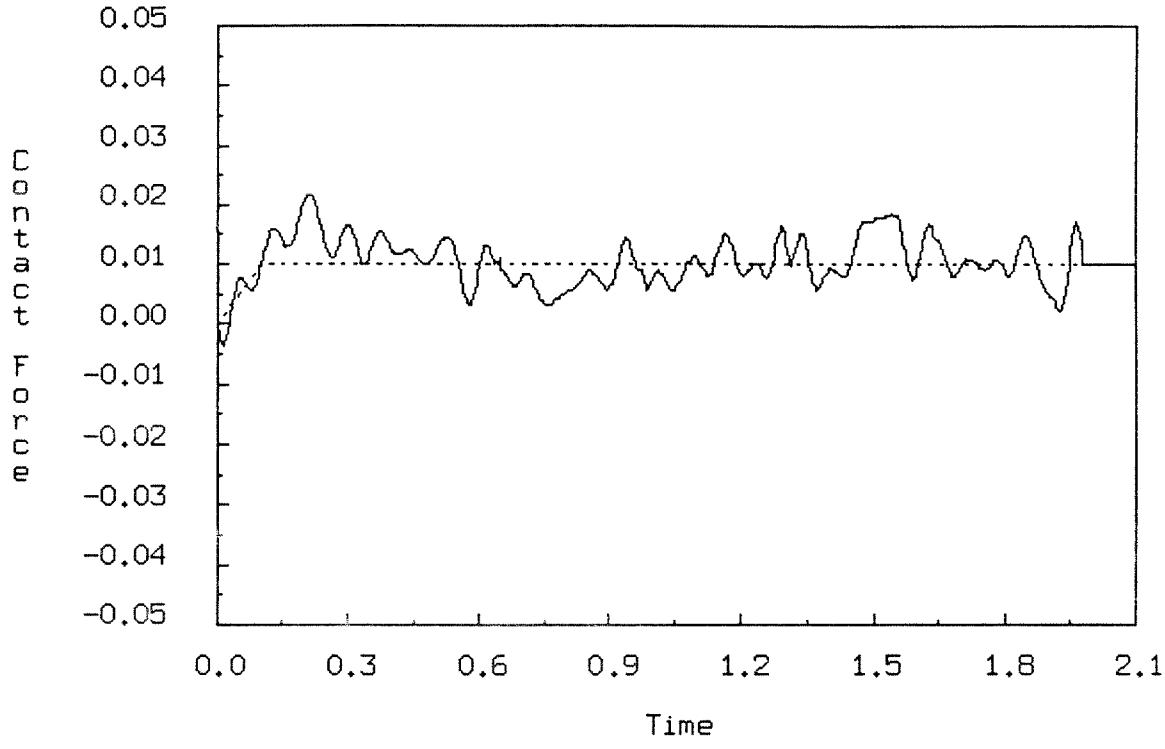

Figure 5.4d. *Effects of braking on vehicle/structure system.* (Nominal motion as unknown.) Horizontal contact force F_c^1 (normalized wrt vertical force $|F^2|$) vs. Time. Solid line: flexible structure. Dotted line: rigid structure. $\dot{Y}^1(0) = 75m/s$.

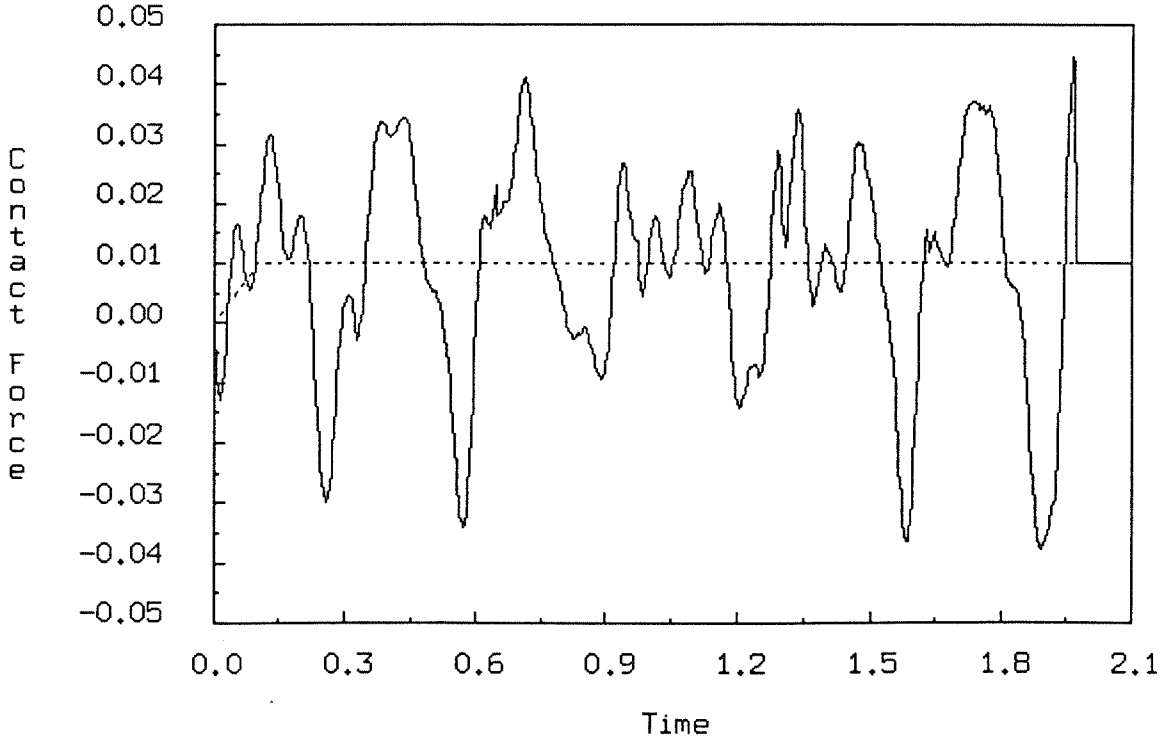

Figure 5.4e. *Effects of braking on vehicle/structure system.* (Nominal motion as on rigid beam.) Horizontal contact force F_c^1 (normalized wrt vertical force $|F^2|$) vs. Time. Solid line: flexible structure. Dotted line: rigid structure. $\dot{Y}^1(0) = 75m/s$.

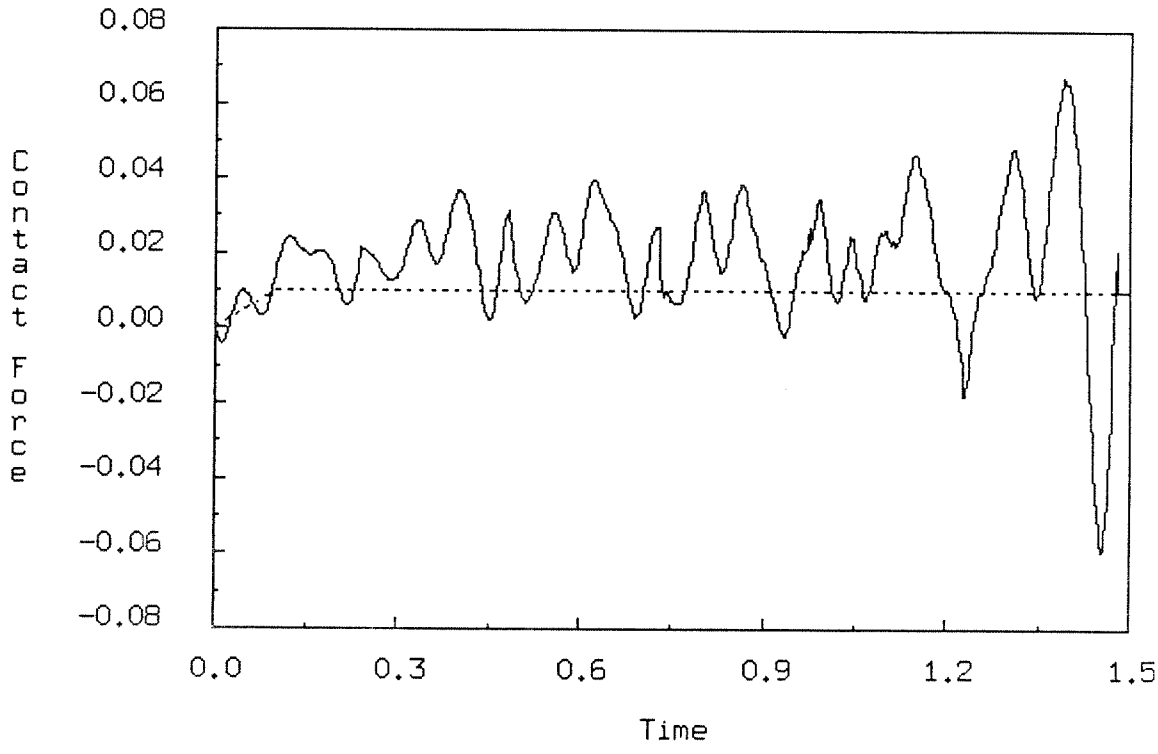

Figure 5.4f. *Effects of braking on vehicle/structure system.* (Nominal motion as unknown.) Horizontal contact force F_c^1 (normalized wrt vertical force $|F^2|$) vs. Time. Solid line: flexible structure. Dotted line: rigid structure. $\dot{Y}^1(0) = 100m/s$.

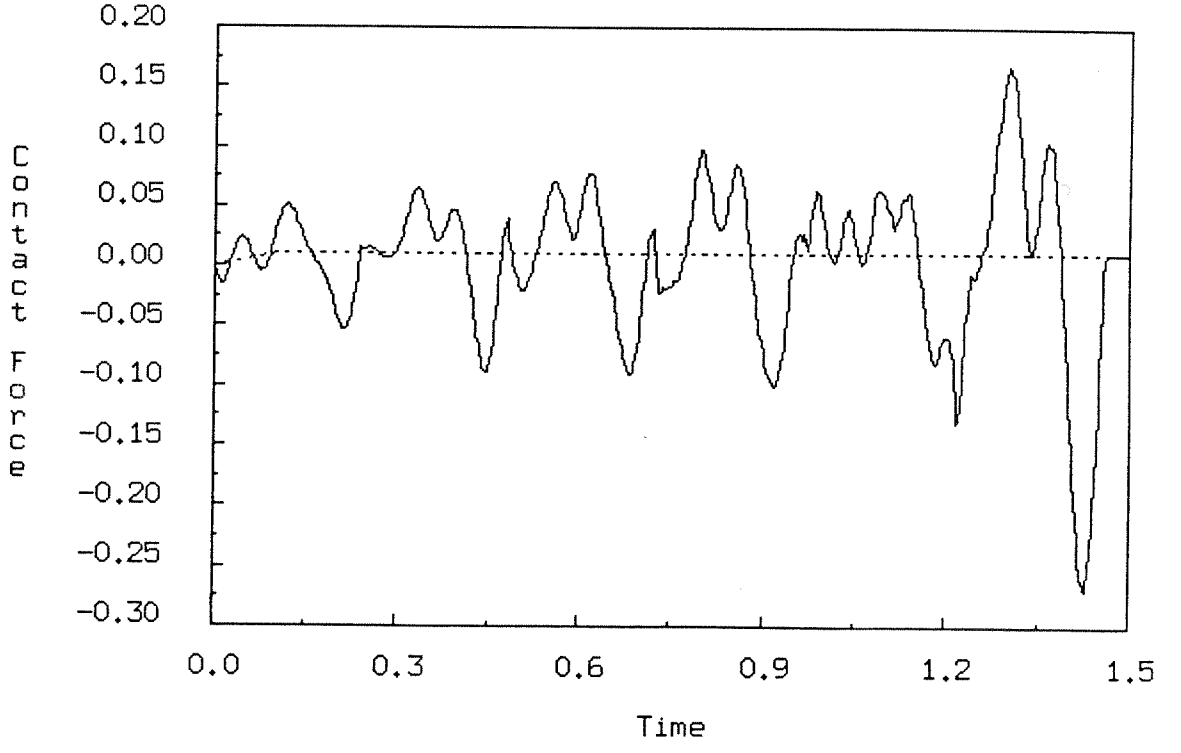

Figure 5.4g. *Effects of braking on vehicle/structure system.* (Nominal motion as on rigid beam.) Horizontal contact force F_c^1 (normalized wrt vertical force $|F^2|$) vs. Time. Solid line: flexible structure. Dotted line: rigid structure. $\dot{Y}^1(0) = 100m/s$.